Apoptosis is mediated through various biochemical steps. One of the best-characterized apoptotic pathways is that induced through the surface molecule Fas (16, 17). Fas agonist causes trimerization of Fas and recruits a number of molecules to form a complex death-inducing signaling complex (DISC), starting with recruitment of the Fas-adapter protein FADD through Fas and FADD's mutual death domains. The other end of FADD contains two death-effector domains (DEDs) that recruit caspase-8 (FLICE) or its enzymatically inactive homologue, the Fas inhibitory FLICE inhibitor protein (FLIP). Procaspase-8 is cleaved and activated after binding to FADD (18–20). This starts the following cascade reactions toward apoptosis. Interestingly, IL-6, which is known to play a crucial role in liver regeneration via Stat3, protects liver against Fas-mediated apoptosis by inducing a critical level of antiapoptotic proteins such as FLIP, Bcl-2, and Bcl-xL (19).

Clinically, Fas has been shown to be important in hepatitis and other liver diseases (21–23). The liver is very sensitive to Fas-mediated apoptosis because Fas antigen is constitutively expressed on hepatocytes. When mice are injected with anti-Fas antibody, death due to liver failure follows (19). *Fas*$^{-/-}$ mice show hepatic hyperplasia, suggesting that the Fas pathway may be important for establishing liver structure and size. The Fas/FasL system seems to be involved in many pathological situations, such as graft-versus-host disease, liver transplant, hepatitis B and C, acute alcoholic hepatitis, and some biliary diseases (21, 23, 24).

The present study was designed to investigate the protective effect of Stat3 against Fas-mediated liver injury. An adenovirally overexpressed, constitutively activated form of Stat3 (Stat3-C) dramatically suppressed Fas-mediated liver injury by upregulating protein levels of FLIP, Bcl-2, Bcl-xL, and redox factor-1 (Ref-1).

Methods

Adenoviral vectors. The Stat3-C construct, which was provided by James E. Darnell (Rockefeller University, New York, USA), was made by substituting cysteine residues for A661 and N663 of murine Stat3 and was tagged with FLAG. This renders the Stat3-C molecule capable of dimerizing without a phosphate on Y705 (25). A replication-deficient adenoviral vector encoding Stat3-C (AxCAS3-C) was constructed in our laboratory. AdLacZ, an adenovirus encoding inert bacterial β-gal, was used as a control vector. AdRef and AdFer, encoding full-length Ref-1 in the sense and antisense directions, respectively, have been reported previously (26).

Animal experiments. C57BL/6 male mice, 6–8 weeks old, were used for the experiments. Adenoviral vectors were injected intravenously via tail vein 3 days prior to experiments (3×10^8 PFU/mouse). In experiments using multiple viral vectors, total amounts of adenoviruses injected were adjusted to 3×10^8 PFU/mouse. After a 24-hour fast, the mice were injected intraperitoneally with Jo2 antibody (0.3 μg/g body wt; BD PharMingen, San Diego, California, USA). In some experiments, *N*-acetyl-L-cysteine (NAC) (200 mg/kg body wt) (27) and the general apoptosis inhibitor Z-VAD-fmk (1 μg/g body wt; Enzyme Systems Products Inc., Livermore, California, USA) (28) were intraperitoneally injected 1 hour prior to the experiment. All animals were handled according to the policies set by the Laboratory Animal Care and Use Committee of The National Research Institute for Child Health and Development.

Experiments using primary cultured hepatocytes. Primary cultured hepatocytes were prepared by a conventional collagenase perfusion method from C57BL/6 mouse liver. Hepatocytes were seeded at 3×10^6 cells per 10-cm dish 24 hours prior to adenoviral infection. AdLacZ or AxCAS3-C was infected at an MOI of 2, followed by Jo2 administration at 2.5 μg/ml 48 hours later. Cells were harvested for the analysis of protein expression 48 hours after adenoviral infection, and apoptosis assays were performed 8 hours after Jo2 administration.

Generation of LS3-KO mice. We generated LS3-KO mice by breeding Stat3-flox mice (15) with albumin-Cre transgenic (Alb-Cre) mice (29), which express Cre recombinase specifically in the liver under the control of the albumin promoter. To increase the efficiency of Stat3 disruption, we also introduced a Stat3 null allele over the floxed allele by crossing with Stat3 heterozygous knockout (*Stat3*$^{+/-}$) mice (10). We crossed *Stat3*$^{+/-}$ mice with Alb-Cre mice and generated *Stat3*$^{+/-}$, Alb-Cre mice, then bred these mice with mice harboring homozygous Stat3 floxed allele (*Stat3*$^{flox/flox}$). The resulting *Stat3*$^{flox/-}$, Alb-Cre mice were used as LS3-KO mice. *Stat3*$^{flox/-}$ mice obtained from the same breeding were used as control mice.

Western blot analysis. The liver homogenates were centrifuged and the supernatants were used for the assay. Fifty micrograms of protein was used for 15% SDS-PAGE. The protein transferred to the nitrocellulose membrane was incubated with the proper antibodies, anti-Fas, anti–Bcl-2, anti–Bcl-xL, anti-Survivin (Santa Cruz Biotechnology Inc., Santa Cruz, California, USA), anti–FLIP-CT (Cell Signaling Technology Inc., Beverly, Massachusetts, USA), anti-Ref-1, anti–manganese superoxide dismutase (anti-MnSOD; Transduction Laboratories, San Diego, California, USA), anti-thioredoxin (BD PharMingen), and anti-FLAG (Sigma-Aldrich, St. Louis, Missouri, USA).

Electrophoretic mobility shift assay. Stat3 DNA binding activity was assayed using the SIE-m67 oligonucleotide as a probe (5′-actgGGATTTTTCCCGTAAATGGTC-3′). The reaction mixture contained nuclear protein extract (5 μg), DTT (2 mM), dI-dC (2 μg), ssDNA (10 μg/ml), and ^{32}P-labeled SIE-m67 probe (5×10^5 cpm). The specimens were electrophoresed on 5% polyacrylamide native gels at 4°C in 0.25 × Tris-Borate/EDTA (TBE) buffer.

Histological studies. Liver tissue was excised and fixed with 10% buffered formalin, and paraffin-embedded sections were stained with H&E. For immunohistochemical demonstration of Stat3 protein, specimens were incubated with primary antibody (anti-Stat3; BD Transduction Laboratories, Lexington, Kentucky, USA)

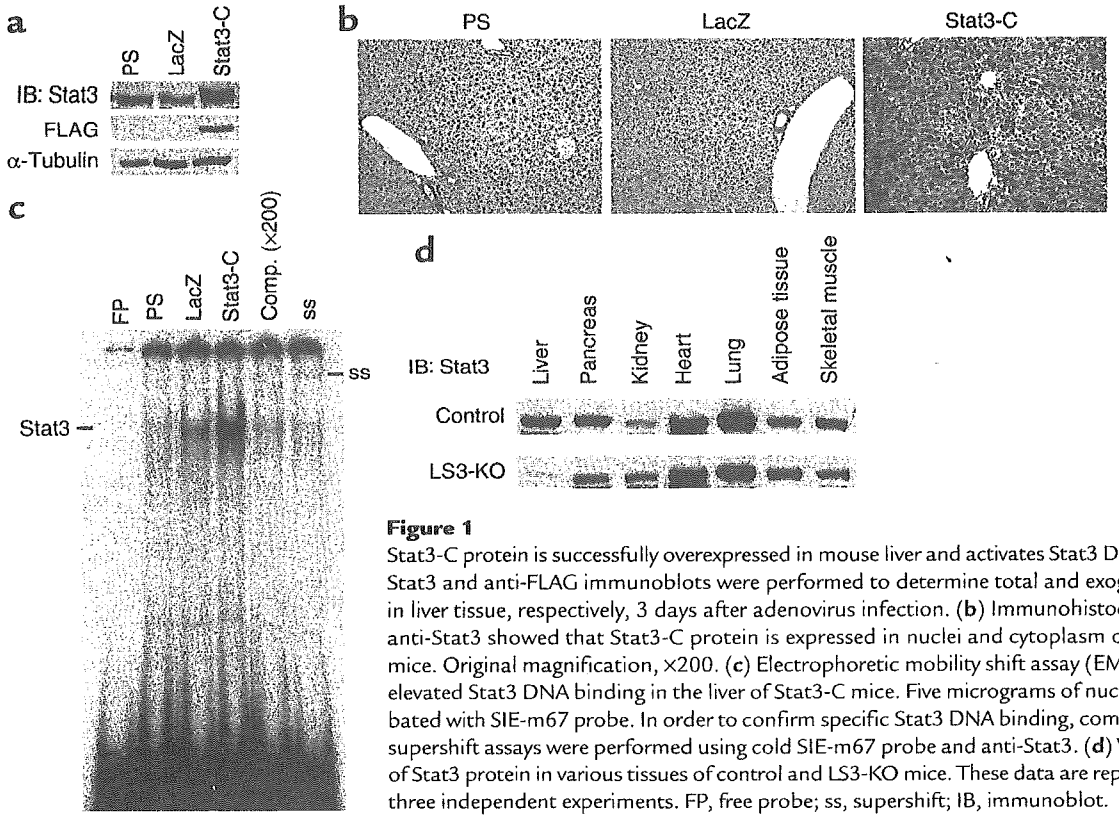

Figure 1

Stat3-C protein is successfully overexpressed in mouse liver and activates Stat3 DNA binding. (**a**) Anti-Stat3 and anti-FLAG immunoblots were performed to determine total and exogenous Stat3 protein in liver tissue, respectively, 3 days after adenovirus infection. (**b**) Immunohistochemical study using anti-Stat3 showed that Stat3-C protein is expressed in nuclei and cytoplasm of the liver in Stat3-C mice. Original magnification, ×200. (**c**) Electrophoretic mobility shift assay (EMSA) analysis showed elevated Stat3 DNA binding in the liver of Stat3-C mice. Five micrograms of nuclear extract was incubated with SIE-m67 probe. In order to confirm specific Stat3 DNA binding, competition (comp.) and supershift assays were performed using cold SIE-m67 probe and anti-Stat3. (**d**) Western blot analysis of Stat3 protein in various tissues of control and LS3-KO mice. These data are representative of at least three independent experiments. FP, free probe; ss, supershift; IB, immunoblot.

at 2.5 μg/ml at 4°C overnight, followed by the secondary antibody (biotin-conjugated anti-mouse IgG).

Apoptosis assay. The In situ Cell Death Detection Kit (Roche Diagnostics Corp., Basel, Switzerland) was used for the demonstration of apoptotic cell death of the liver tissue. Paraffin-embedded liver specimens were incubated with the TUNEL reaction mixture according to manufacturer's recommendations. Also, Cell Death Detection ELISA PLUS (Roche Diagnostics Corp.) was used for the quantitative evaluation of apoptotic cells. Lysates of liver tissue were directly applied for this assay (40 μg of protein), and the assay was performed according to the manufacturer's recommendations.

Caspase activity assay. Activities of caspase-3, -8, and -9 were measured using the CPP32/Caspase-3 Colorimetric Protease Assay Kit, FLICE/Caspase-8 Colorimetric Protease Assay Kit, and Caspase-9/Mch6 Colorimetric Protease Assay Kit, respectively, from Medical and Biological Laboratories Co. (Tokyo, Japan). Supernatant of liver homogenate was prepared (200 μg in 50 μl) and reacted with the substrate at 37°C for 1 hour prior to the assay.

Hepatic reactive oxygen species assay in liver tissue. Production of reactive oxygen species (ROS) in liver tissue was measured by two independent methods, lucigenin-enhanced chemiluminescence and hydrogen peroxide assays, the details of which were described previously (30). After isolating hepatocytes by conventional perfusion methods, 100 μl of cell suspension (10^5 cells) was added to 1 ml of lucigenin buffer (75 mM lucigenin in HBSS). The chemiluminescent signal was monitored every 5 minutes for 30 minutes. The emitted light units (after subtracting a blank and integrating over 15 minutes) were used as a measure of superoxide production. Hydrogen peroxide production was measured using the Amplex Red Hydrogen Peroxide Assay Kit (Molecular Probes Inc., Eugene, Oregon, USA). Supernatant of liver homogenate was used for the assay, according to the manufacturer's recommendations. After subtraction of a blank sample, the red fluorescence signal was standardized by protein concentration, and hydrogen peroxide concentration (expressed as mmol/mg protein) was calculated based on a standard curve.

Analysis of mRNA. For multiprobe ribonuclease protection assay, the presence of transcripts of the indicated genes and the internal control *L32* were detected using a multiprobe template set (BD PharMingen). Probe synthesis, hybridization, and RNase treatment were performed according to the manufacturer's recommendations. The protected transcripts were resolved by electrophoresis on denaturing 4.75% polyacrylamide gels and quantified on a PhosphorImager (Amersham Biosciences, Piscataway, New Jersey, USA). For Northern blot analysis, total cellular RNA was extracted and electrophoresed on a 1.4% agarose gel. RNA was transferred to a nylon membrane, which was hybridized with 3×10^7 cpm of ^{32}P-labeled single-strand Ref-1 cDNA. After washing, the membrane was autoradiographed.

Transient transfection experiments and luciferase reporter assay. The human *Ref-1* promoter was cloned by PCR from HeLa genomic DNA as previously reported (31, 32) and cloned into pGL3 (Promega Corp., Madison, Wisconsin, USA). HeLa cells were seeded at a density of $1.5 \times 10^4/cm^2$, and LipofectAMINE (Invitrogen Corp., Carlsbad, California, USA) was used as the transfectant according to the manufacturer's recommendations. Forty-eight hours after transfection of *Ref-1* promoter gene, adenoviral vector was infected at various MOI as indicated. Luciferase activity was assessed 36 hours after adenovirus infection using the Bright-Glo luciferase assay system (Promega Corp.) according to the manufacturer's recommendations. Results of each reporter assay were reproducible in three separate experiments.

Statistical analysis. Fisher's test was used for analysis of differences between multiple groups and was considered significant at the 95% confidence level. The number of animals (n) used for each experiment is indicated in parentheses.

Results

Expression and activity of Stat3 in liver of mice injected with AxCAS3-C and of LS3-KO mice. DNA binding. Adenoviral vector (1×10^8 PFU/mouse) encoding a constitutively activated form of the *Stat3* gene (AxCAS3-C) was intravenously injected into mice 3 days prior to the experiment. This successfully overexpressed a constitutively activated form of Stat3 protein (Stat3-C) in mouse liver (Figure 1, a and b). Immunoblot and immunohistochemical analyses using anti-Stat3 demonstrated that the amount of total Stat3 protein in the liver of mice infected with AxCAS3-C (Stat3-C mice) was higher than that in mice injected with physiological saline (PS mice) and AdLacZ (LacZ mice). The expression of exogenously expressed Stat3-C protein was also confirmed by anti-FLAG in the liver of Stat3-C mice (Figure 1a). Immunohistochemical analysis revealed that Stat3-C protein was expressed in both the cytoplasm and nucleus in the liver of Stat3-C mice, though Stat3 protein was hardly detected in the liver of PS and LacZ mice (Figure 1b). Stat3-C resulted in no abnormality observed in the hepatic structure.

Stat3 DNA binding was not activated in the PS mouse liver in quiescent conditions. Overexpression of Stat3-C resulted in strong activation of its DNA binding, whereas AdLacZ infection only partially activated Stat3 DNA binding (Figure 1c).

In the liver of LS3-KO mice, the amount of Stat3 protein was less than 5% of that of *Stat3*$^{flox/-}$ mice, whereas various other tissues including pancreas, kidney, heart, lung, adipose tissue, and skeletal muscle did not differ in Stat3 expression between control and LS3-KO mice (Figure 1d).

Stat3-C prevents liver injury induced by Fas agonist. Expression of Stat3-C resulted in a liver that was macroscopically normal in size and color with microscopic mild

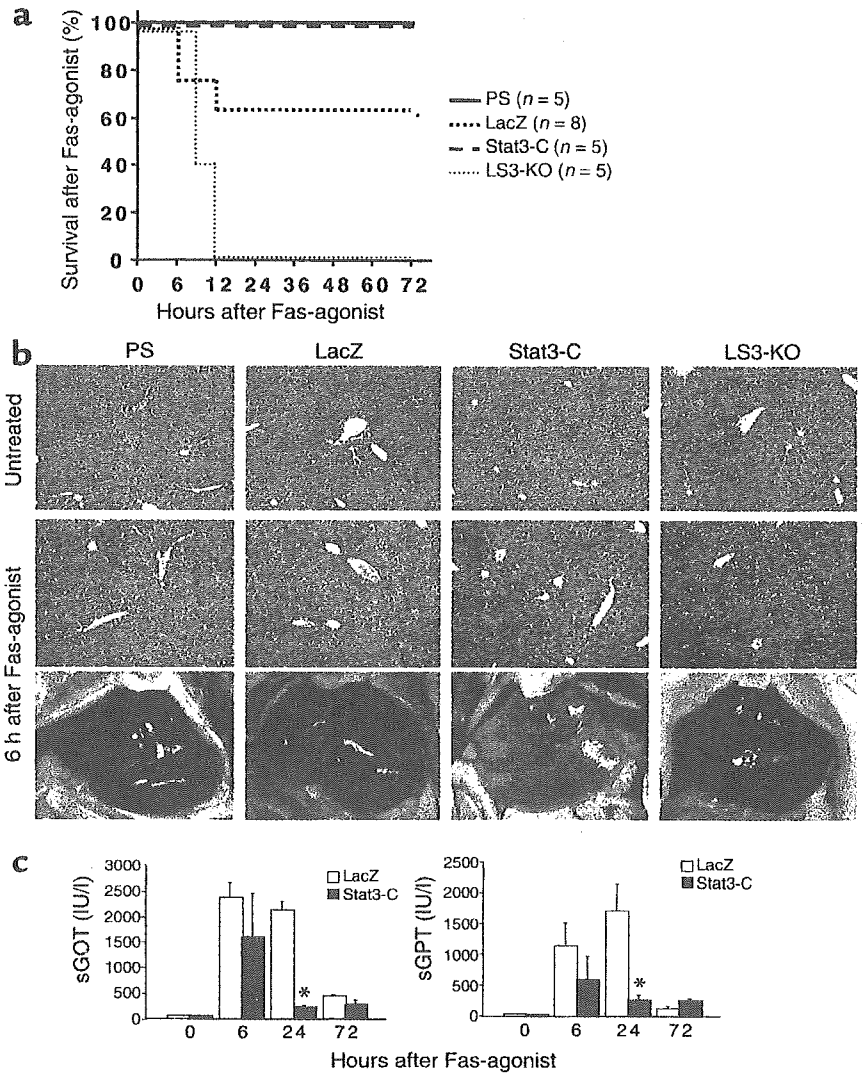

Figure 2
Stat3-C prevents liver injury induced by Fas agonist. (**a**) Survival after Fas agonist treatment. Mice were injected intraperitoneally with Jo2 (0.3 μg/g body wt) and followed for 72 hours. (**b**) Liver appearance and microscopic change 6 hours after Fas agonist. H&E staining; original magnification, ×100. (**c**) Serum levels of GOT and GPT (sGot and sGPT) until 72 hours after Fas agonist treatment. *$P \leq 0.01$ vs. LacZ 24 hours after treatment with Fas agonist. Data are expressed as mean ± SEM (n = 5).

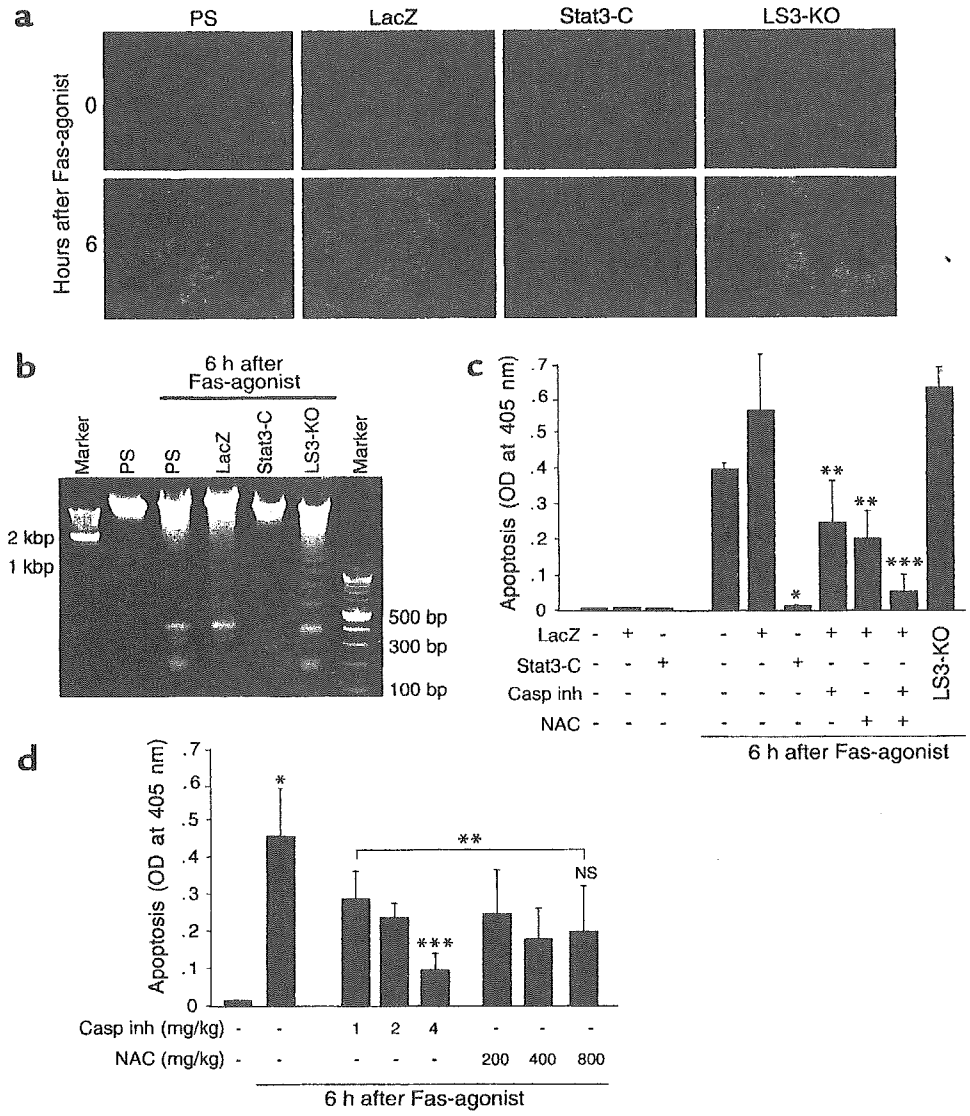

Figure 3
Stat3-C suppresses Fas-induced apoptotic cell death in liver. (**a**) Fluoromicroscopic photographs of liver sections with TUNEL staining from PS, LacZ, Stat3-C, and LS3-KO mice treated with Fas agonist (formalin-fixed, paraffin-embedded sections; original magnification, ×100). (**b**) The DNA ladder pattern was analyzed 6 hours after Fas agonist. Each photo is representative of at least three independent experiments. (**c**) Apoptotic cell death was quantitatively measured by ELISA. Pretreatment with the general caspase inhibitor Z-VAD-fmk (1 μg/g body wt) or the antioxidant NAC (200 mg/kg body wt) was performed 1 hour prior to the experiments. $*P < 0.01$ vs. LacZ/Fas agonist, $**P < 0.05$ vs. LacZ/Fas agonist and Stat3-C/Fas agonist, $***P < 0.05$ vs. LacZ/Fas agonist + caspase inhibitor and LacZ/Fas agonist + NAC. (**d**) Dose-dependent effects of caspase inhibitor (Z-VAD-fmk) or antioxidant (NAC) upon hepatic apoptosis after Fas agonist. $*P < 0.01$ vs. untreated control, $**P < 0.05$ vs. Fas agonist, $***P < 0.05$ vs. Fas agonist + caspase inhibitor (1 and 2 mg/kg, respectively). All data are expressed as mean ± SEM ($n = 5$). Casp inh, caspase inhibitor.

inflammatory cell infiltration 3 days after viral injection. Intraperitoneal injection of Jo2 at 0.3 μg/g body wt induced severe liver injury, but did not show lethality until 72 hours after injection in PS mice and Stat3-C mice. Though three of eight LacZ mice could not survive over 12 hours, LS3-KO mice showed absolute lethality at 12 hours after Jo2 injection (Figure 2a).

At 6 hours following Jo2 injection, the liver turned dark red in color, though the mice were still alive. Histological examination revealed massive hepatic hemorrhage with necrosis at 6 and 24 hours after injection and severe neutrophilic infiltration at 72 hours after injection (Figure 2b). Stat3-C expression markedly reduced Fas-mediated liver injury. Liver was architecturally preserved with sporadic reddish changes in appearance, and microscopically much less bleeding and necrosis were observed 6 hours and 24 hours after Jo2 injection.

Serum levels of glutamic-oxaloacetic transaminase (GOT) and glutamic-pyruvic transaminase (GPT) were remarkably raised 6 and 24 hours after Jo2 injection in LacZ mice. This increase, however, was dramatically reduced in Stat3-C mice (Figure 2c). These data clearly demonstrate that Stat3-C confers resistance against Fas-mediated liver injury.

Stat3-C prevents apoptosis induced by Fas agonist. To confirm antiapoptotic properties of Stat3, hepatic apoptosis induced by Jo2 was studied by three independent methods: TUNEL staining of histological sections, DNA ladder assay, and ELISA (Figure 3, a–c). Massive apoptotic cell death observed 6 hours after Jo2 injection in livers of PS, LacZ, and LS3-KO mice was dramatically reduced by Stat3-C expression. A typical DNA ladder pattern was also identified in specimens from PS, LacZ, and LS3-KO mice (Figure 3b).

Interestingly, pretreatment with the general caspase inhibitor Z-VAD-fmk (1 μg/g) or the antioxidant NAC (200 mg/kg) inhibited Jo2-induced hepatic apoptosis significantly, but failed to inhibit it completely even with increased amounts of these reagents (Figure 3, c and d). However, when administered together, they suppressed apoptosis more effectively (Figure 3c), with a synergistic suppressive effect almost equal to that of

Stat3-C. These facts may indicate that activated Stat3 suppresses Fas-induced liver injury via caspase-dependent and/or redox-dependent mechanisms.

Antiapoptotic proteins are induced in liver expressing Stat3-C. To address the antiapoptotic mechanism of Stat3 acting upon Fas-mediated liver injury, we first investigated the expression of apoptosis-related proteins (Figure 4a). Overexpressed Stat3-C did not suppress hepatic Fas expression, but upregulated it. Infection with AdLacZ, however, induced Fas to the same degree as was observed in Stat3-C mice. Stat3-C upregulated Bcl family proteins with antiapoptotic properties (Bcl-xL and Bcl-2), whereas adenovirus itself did not induce these proteins. Jo2 injection induced Fas and Bcl-xL proteins

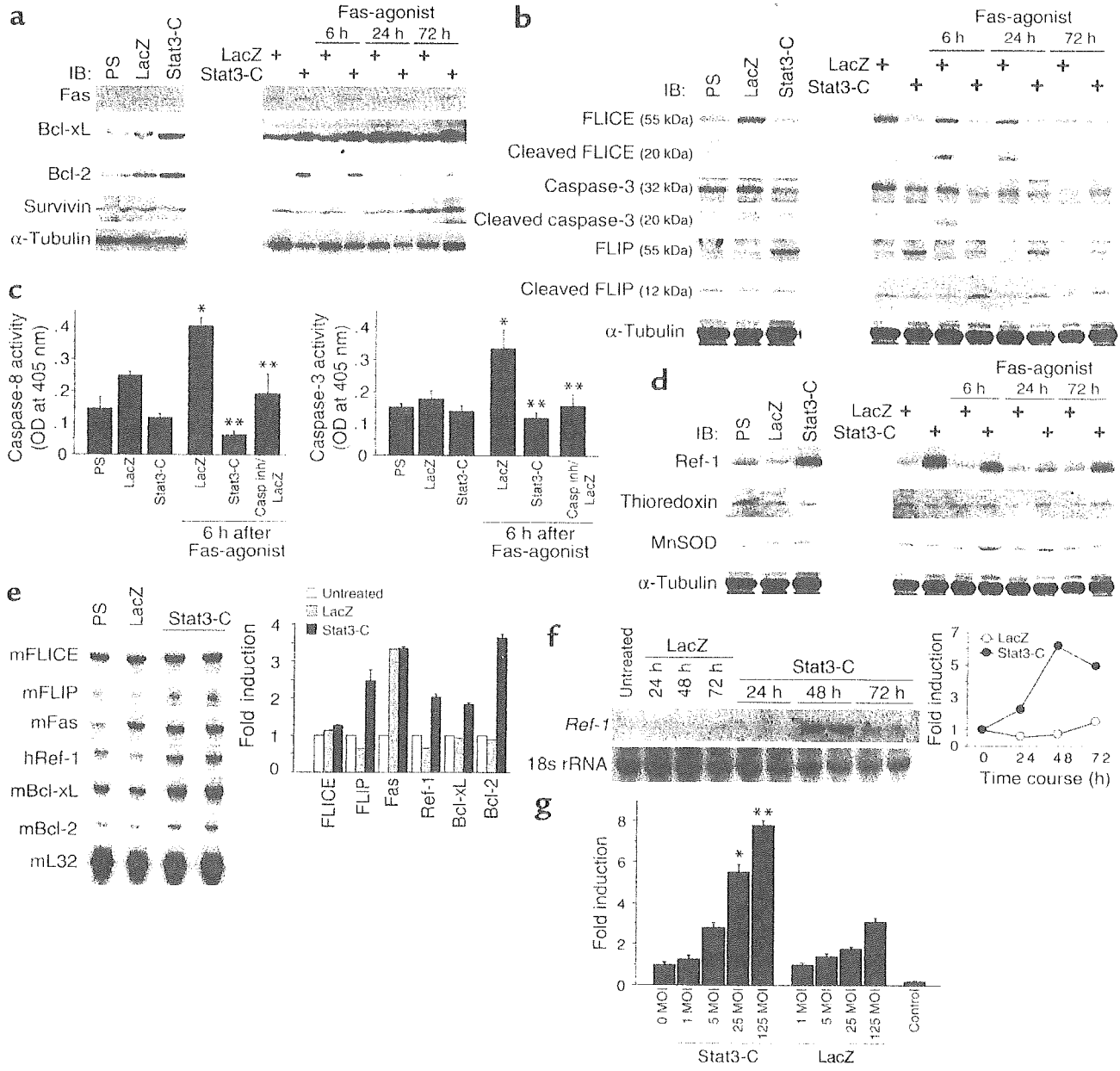

Figure 4

Stat3-C induces apoptosis-related proteins and redox-related protein. Immunoblot, Northern blot, and multiprobe ribonuclease protection assay were performed on liver tissues from PS, LacZ, and Stat3-C mice. Sequential changes of the protein amounts after Fas agonist treatment were analyzed in LacZ and Stat3-C mice. Each blot is representative of three independent experiments. (**a**) Expression of Fas, Bcl-related proteins, and Survivin. (**b**) Expression of caspase-related proteins. (**c**) Enzyme activity assays of caspase-3 and caspase-8. $*P < 0.05$ vs. LacZ, $**P < 0.01$ vs. LacZ/Fas agonist. (**d**) Protein expression of redox-related proteins Ref-1, thioredoxin, and MnSOD. (**e**) Multiprobe ribonuclease protection assay for apoptosis-related genes and redox-related genes 48 hours after adenoviral gene transfer. m, mouse; h, human. (**f**) Northern blot analysis for *Ref-1* mRNA after adenoviral gene transfer of *Stat3-C*. Results are from a single representative experiment that was reproduced once (**d**–**f**). (**g**) Transcriptional activity of *Ref-1* promoter by Stat3-C. Luciferase assay for *Ref-1* promoter activity stimulated by AxCAS3-C or AdLacZ. Control was pGL3 without *Ref-1* promoter. $*P \leq 0.01$ vs. uninfected (0 MOI, 0) and LacZ (25 MOI), $**P \leq 0.01$ vs. uninfected (0 MOI) and LacZ (125 MOI). All data are expressed as mean ± SEM ($n = 5$).

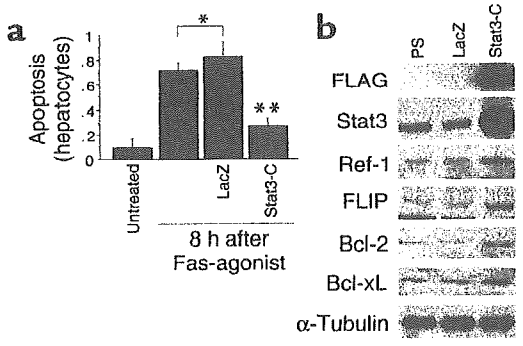

Figure 5
Stat3-C protects primary hepatocytes from Jo2-induced apoptosis with significant expression of apoptosis- and antioxidant-related proteins in hepatocytes. (**a**) Apoptotic cell death of primary hepatocytes was quantitatively measured by ELISA. $*P < 0.05$ vs. untreated, $**P < 0.01$ vs. LacZ/Fas agonist. All data are expressed as mean ± SEM ($n = 5$). (**b**) Protein expression by Stat3-C in primary hepatocytes.

24 hours after injection in LacZ mice. Stat3-C did not alter the expression of Survivin protein, which is reported to be induced by Stat3 in some types of cells (13).

FLIP protein is induced and activated by Stat3-C followed by reduction of FLICE and caspase-3 activities. Stat3-C suppressed expression of FLICE protein as well as caspase-3 (albeit to a lesser extent), as determined by comparing Stat3-C mice with PS and LacZ mice. Though FLICE and caspase-3 were both processed and activated 6 hours after Jo2 injection in LacZ mice, Stat3-C inhibited both expression and activation of these proteins by Fas agonist (Figure 4, b and c). FLIP protein was also induced by Stat3-C, but not by PS and LacZ, and was significantly activated following Jo2 injection until 72 hours afterward (Figure 4b). IL-6, one of the major ligands for Stat3, has already been reported to upregulate FLIP, Bcl-2, and Bcl-xL in liver (19). Interestingly, Stat3-C suppressed caspase activity to the same degree as caspase inhibitor did, if not more (Figure 4c). These data may suggest that Stat3 plays a critical role in IL-6–associated antiapoptotic activity in liver.

Stat3-C induces redox-related protein Ref-1. Because pretreatment with an antioxidant, NAC, partially improved Fas-mediated hepatic apoptosis (Figure 3c), we next investigated the expression of redox-related proteins in liver overexpressing Stat3-C. Protein expression of Ref-1 was remarkably upregulated by Stat3-C prior to Jo2 injection, though it was slightly downregulated by LacZ (Figure 4d). The increased amount of Ref-1 protein was reduced following Jo2 injection. In support of this, Stat3-C induced *Ref-1* transcript 48–72 hours after AxCAS3-C injection (see Figure 4f), though it was not detected at all in livers injected with PS and AdLacZ. However, Stat3-C had no effect on the

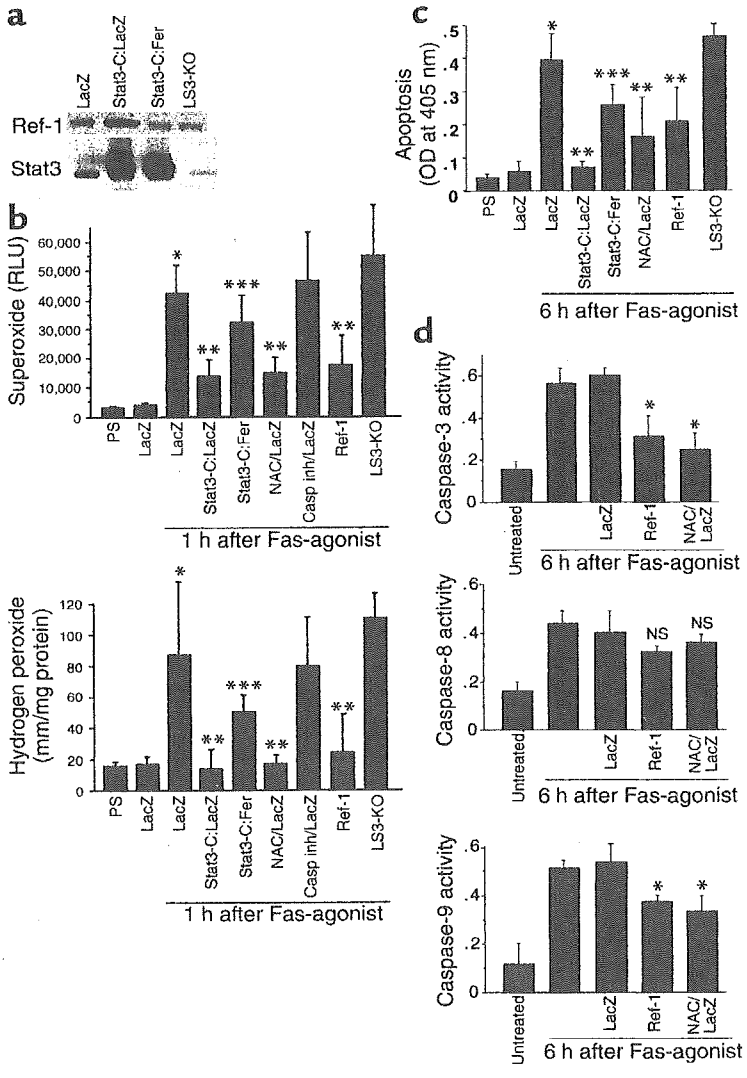

Figure 6
Hepatic ROS production and apoptosis induced by Fas agonist are suppressed by Stat3-C via Ref-1. LacZ, Stat3-C:LacZ, and Stat3-C:AdFer (Stat3-C:Fer) mice were infected with AdLacZ only, AxCAS3-C:AdLacZ (1:1), and AxCAS3-C:AdFer (1:1), respectively. Total amounts of adenovirus vectors were adjusted to 3×10^8 PFU/mouse in all experiments. (**a**) Immunoblots of Ref-1 and Stat3 proteins showing that AxCAS3-C increased Stat3 and Ref-1 proteins, but AdFer reduced them. Ref-1 protein was, however, expressed even in the liver of LS3-KO mice. (**b**) Superoxide generation assay and hydrogen peroxide assay in liver tissue $*P < 0.05$ vs. LacZ, $**P < 0.05$ vs. LacZ/Fas agonist, $***P < 0.05$ vs. Stat3-C:LacZ/Fas agonist. Casp inh; i.e. Z-VAD-fmk. (**c**) Apoptotic cell death was quantitatively analyzed by ELISA. $*P < 0.01$ vs. LacZ, $**P < 0.05$ vs. LacZ/Fas agonist, $***P < 0.05$ vs. Stat3-C:LacZ/Fas agonist. (**d**) Enzyme activity assays of caspase-3 and caspase-8. $*P < 0.05$ vs. LacZ/Fas agonist. All data are expressed as mean ± SEM ($n = 5$). RLU, relative light unit.

amounts of two other redox-related proteins, thioredoxin and MnSOD (Figure 4d). MnSOD was transiently increased after Jo2 injection in liver overexpressing Stat3-C, which may provide evidence for an oxidant-dependent mechanism in Fas-mediated liver injury. These findings indicate that activated Stat3 specifically upregulates Ref-1 in mouse liver.

Transcriptional upregulation of proteins associated with Stat3. Ribonuclease protection assay revealed that, 48 hours after adenoviral gene transfer, the level of *Fas* mRNA was elevated by LacZ and Stat3-C, and *Bcl-xL*, *Bcl-2*, *FLIP*, and *Ref-1* mRNAs were all elevated only by Stat3-C (Figure 4e). The level of *FLICE* mRNA, however, was not changed at all by LacZ and Stat3-C. We also confirmed *Ref-1* mRNA expression by Northern blot analysis, because Ref-1 may play crucial roles in suppressing liver injury with its antioxidant and antiapoptotic properties (26). Stat3-C increased *Ref-1* mRNA levels 48–72 hours after AxCAS3-C infection prior to Ref-1 protein expression (Figure 4f), though it hardly detected in livers injected with PS and AdLacZ.

In order to see whether Ref-1 is transcriptionally upregulated by Stat3-C, activation of *Ref-1* promoter by Stat3 was also measured. Although AdLacZ moderately stimulated Ref-1 promoter activity, Stat3-C markedly stimulated the activity in a dose-dependent manner (Figure 4g).

Effects of Stat3 upon primary hepatocytes. To examine whether Stat3-C directly targets hepatocytes or not, we performed experiments using primary cultured mouse hepatocytes. Exogenous Stat3-C was successfully expressed by infection of AxCAS3-C at an MOI of 2 in primary hepatocytes, and reduced Fas-induced apoptosis (Figure 5, a and b). Stat3-C treatment resulted in overexpression of Ref-1, FLIP, Bcl-2, and Bcl-xL proteins in primary hepatocytes as well as in liver. This indicates that Stat3 directly targets at least hepatocytes and may have antiapoptotic and antioxidant effects upon hepatocytes.

Stat3-C reduces hepatic ROS production and apoptosis through Ref-1. Adenoviral vector encoding antisense full-length *Ref-1* gene (AdFer) was injected into the mice in order to investigate the role of Ref-1 in the hepatic generation of ROS and Fas-mediated liver injury. The amount of Ref-1 protein was increased in Stat3-C mice coinfected with AdLacZ, but was reduced in Stat3-C mice coinfected with AdFer (Figure 6a). Hepatic ROS were produced 1 hour after Jo2 injection; these were reduced by overexpression of Stat3-C and Ref-1, and by pretreatment with NAC. ROS production, however, was not affected by caspase inhibitor alone. This antioxidant effect of Stat3-C was partially reversed by coinfection with AdFer. Stat3-C was considered to have an antioxidant effect through induction of Ref-1 (Figure 6b). Jo2-induced hepatic apoptosis was suppressed by pretreatment with NAC as well as Stat3-C. As expected, the suppression of apoptosis by Stat3-C was also reduced by AdFer coinfection (Figure 6c). Assays of caspase activities revealed that Ref-1 and NAC equally reduced caspase-3 activity and partially reduced caspase-9 activity induced by Jo2 injection, but did not reduce caspase-8 activity (Figure 6d). Ref-1 may have reduced caspase activities (caspase-3 and -9) by reducing oxidative stress. These facts suggest that Stat3 possesses redox-dependent antiapoptotic properties through inactivation of caspase-3 and -9 resulting from increased Ref-1 expression.

Discussion

This study reports on the protective effects of an activated form of Stat3 against Fas-mediated liver injury and the underlying mechanisms of these effects (Figure 7). One of the major protective mechanisms against Fas-induced apoptosis in mouse liver seems to be a caspase-dependent mechanism. Stat3-C suppressed hepatic apoptosis through inhibition of both caspase-8 and -3 activities via upregulation of FLIP protein and through upregulation of Bcl-2 and Bcl-xL proteins. The protective effect of Stat3 against apoptosis has already been explained partly by upregulation of antiapoptotic proteins such as Bcl-xL and Survivin (13). IL-6, one of the major ligands for Stat3, is also reported to suppress liver injury of various causes (19, 33–35). Adenovirally overexpressed "hyper IL-6," a fusion protein of IL-6 and its soluble receptor, reversed fulminant liver failure induced by D-galactosamine and also accelerated liver regeneration (35). IL-6 also inhibits Fas-mediated liver injury through upregulation of Bcl-2, Bcl-xL, and FLIP proteins (19). These reports may support our present data.

There are accumulating data indicating that ROS are involved in Fas-mediated apoptosis in various cells (36–39). In the present study, the antioxidant NAC also reduced hepatic generation of ROS and activity of caspase-3 and -9, and prevented the liver from injury

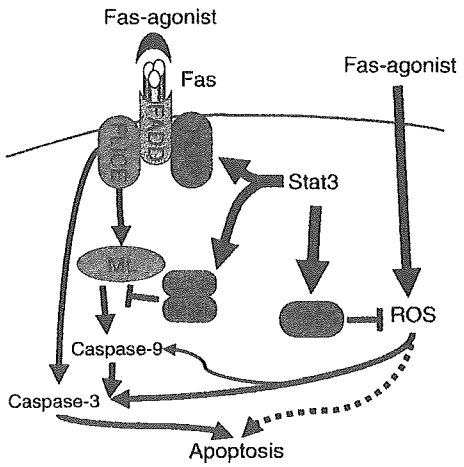

Figure 7
Schematic view of the protective mechanisms of Stat3 against Fas-mediated liver injury. Activation of Stat3 upregulates caspase-related proteins (such as FLIP, Bcl-xL, and Bcl-2) and redox-related protein Ref-1. These proteins collaboratively prevent Fas-mediated liver injury in redox-dependent and/or independent ways. Mt., mitochondria.

induced by Fas agonist. Gulbins et al. have already reported the involvement of Ras-mediated ROS in Fas-mediated cell death (40). Fas may activate caspase activities at least partially via ROS generation and inducing apoptosis, effects that are inhibited by NAC in this pathway.

Interestingly, Stat3 reduced the hepatic generation of ROS following Jo2 administration through upregulation of Ref-1. Ref-1 is primarily a nuclear protein with dual and mutually exclusive nuclear functions: it is an endonuclease in the base excision repair pathway (41) and it is a reducing agent that facilitates the DNA-binding activities of many redox-sensitive transcription factors including NF-κB (26, 42–44). This is a bifunctional protein that is upregulated in response to a host of stimuli that result in intracellular ROS generation (45). Adenovirally overexpressed Ref-1 in mouse liver successfully improves postischemic liver injury through suppression of ROS generation and apoptosis in hepatic tissue (26). This may also explain its role in the Stat3-dependent protection against Fas-induced oxidative liver injury through Ref-1. Stat3-C did not induce other redox-related proteins such as thioredoxin and MnSOD in the present study, though MnSOD induced by Stat3 protects cardiomyocytes against hypoxia/reoxygenation-induced injury (46). In the present study, activities of caspase-3 and caspase-8 were both reduced by Stat3-C. The underlying mechanisms of this effect may involve the direct upregulation by Stat3-C of caspase-associated antiapoptotic proteins such as FLIP, Bcl-2, Bcl-xL, and also caspase-3 inactivation via upregulation of Ref-1.

In this way, Stat3 may play crucial roles in protection against Fas-mediated liver injury. However, very interestingly, hepatic ROS generation and apoptosis were almost the same in control and LS3-KO mice. There may also exist in the cell compensatory mechanisms other than those dependent on Stat3 that are not yet known.

PKB (Akt), a serine-threonine kinase, possesses mitogenic and antiapoptotic actions in endothelial cells when stimulated by HGF (47). Also, we have recently reported that Akt phosphorylates and inactivates the small GTPase Rac1, which results in the reduction of oxidative stress and apoptosis induced by hypoxia/reoxygenation in hepatocytes (48). Ping et al. have reported that cardiac-specific transgenic activation of PKC-ε confers cardioprotection to the ischemic heart (49). These data suggest that some mitogenic signaling molecules may possess antioxidant and/or antiapoptotic properties, and may also support our present data.

Stat3 is one of the most important transcription factors and plays important roles in the initiation of liver regeneration. Though Stat3's effects upon cell cycle–related genes have been extensively studied, antiapoptotic effects and mechanisms of Stat3 have not been well studied. This study is the first to report that Stat3 protects against Fas-mediated hepatic apoptosis by its direct effects on caspase activity with antioxidant effects through Ref-1.

Acknowledgments

We are grateful to James E. Darnell for Stat3-C cDNA and for his critical review, to Seiichi Suzuki for encouragement, and to Mika Kamekawa for her excellent technique in immunohistochemical staining. We also thank Jurg Tschopp for mouse FLIP cDNA.

1. Darnell, J.E., Jr. 1997. STATs and gene regulation. *Science.* **277**:1630–1635.
2. Schuringa, J.J., Jonk, L.J., Dokter, W.H., Vellenga, E., and Kruijer, W. 2000. Interleukin-6-induced STAT3 transactivation and Ser727 phosphorylation involves Vav, Rac-1 and the kinase SEK-1/MKK-4 as signal transduction components. *Biochem. J.* **347**:89–96.
3. Leu, J.I., Crissey, M.A., Leu, J.P., Ciliberto, G., and Taub, R. 2001. Interleukin-6-induced STAT3 and AP-1 amplify hepatocyte nuclear factor 1-mediated transactivation of hepatic genes, an adaptive response to liver injury. *Mol. Cell. Biol.* **21**:414–424.
4. Schuringa, J.J., van der Schaaf, S., Vellenga, E., Eggen, B.J., and Kruijer, W. 2002. LIF-induced STAT3 signaling in murine versus human embryonal carcinoma (EC) cells. *Exp. Cell Res.* **274**:119–129.
5. Levy, D.E., and Lee, C.K. 2002. What does Stat3 do? *J. Clin. Invest.* **109**:1143–1148. doi:10.1172/JCI200215650.
6. Zhong, Z., Wen, Z., and Darnell, J.E. 1994. Stat3: a STAT family member activated by tyrosine phosphorylation in response to epidermal growth factor and interleukin-6. *Science.* **264**:95–98.
7. Lutticken, C., et al. 1994. Association of transcription factor APRF and protein kinase Jak1 with the interleukin-6 signal transducer gp130. *Science.* **263**:89–92.
8. Hirano, T., Ishihara, K., and Hibi, M. 2000. Roles of STAT3 in mediating the cell growth, differentiation and survival signals relayed through the IL-6 family of cytokine receptors. *Oncogene.* **19**:2548–2556.
9. Bowman, T., Garcia, R., Turkson, J., and Jove, R. 2000. STATs in oncogenesis. *Oncogene.* **19**:2474–2488.
10. Takeda, K., et al. 1997. Targeted disruption of the mouse Stat3 gene leads to early embryonic lethality. *Proc. Natl. Acad. Sci. U. S. A.* **94**:3801–3804.
11. Li, W., Liang, X., Kellendonk, C., Poli, V., and Taub, R. 2002. STAT3 contributes to the mitogenic response of hepatocytes during liver regeneration. *J. Biol. Chem.* **277**:28411–28417.
12. Debonera, F., et al. 2001. Activation of interleukin-6/STAT3 and liver regeneration following transplantation. *J. Surg. Res.* **96**:289–295.
13. Shen, Y., Devgan, G., Darnell, J.E., and Bromberg, J.F. 2001. Constitutively activated Stat3 protects fibroblasts from serum withdrawal and UV-induced apoptosis and antagonizes the proapoptotic effects of activated Stat1. *Proc. Natl. Acad. Sci. U. S. A.* **98**:1543–1548.
14. Grandis, J.R., et al. 2000. Constitutive activation of Stat3 signaling abrogates apoptosis in squamous cell carcinogenesis in vivo. *Proc. Natl. Acad. Sci. U. S. A.* **97**:4227–4232.
15. Takeda, K., et al. 1998. Stat3 activation is responsible for IL-6-dependent T cell proliferation through preventing apoptosis: generation and characterization of T cell-specific Stat3-deficient mice. *J. Immunol.* **161**:4652–4660.
16. Nagata, S. 1999. Fas ligand-induced apoptosis. *Annu. Rev. Genet.* **33**:29–55.
17. Matsumura, H., et al. 2000. Necrotic death pathway in Fas receptor signaling. *J. Cell Biol.* **151**:1247–1256.
18. Siegmund, D., et al. 2001. Fas-associated death domain protein (FADD) and caspase-8 mediate up-regulation of c-Fos by Fas ligand and tumor necrosis factor-related apoptosis-inducing ligand (TRAIL) via a FLICE inhibitory protein (FLIP)-regulated pathway. *J. Biol. Chem.* **276**:32585–32590.
19. Kovalovich, K., et al. 2001. Interleukin-6 protects against Fas-mediated death by establishing a critical level of anti-apoptotic hepatic proteins FLIP, Bcl-2, and Bcl-xL. *J. Biol. Chem.* **276**:26605–26613.
20. Budd, R.C. 2002. Death receptors couple to both cell proliferation and apoptosis. *J. Clin. Invest.* **109**:437–442. doi:10.1172/JCI200215077.
21. Pinkoski, M.J., Brunner, T., Green, D.R., and Lin, T. 2000. Fas and Fas ligand in gut and liver. *Am. J. Physiol. Gastrointest. Liver Physiol.* **278**:G354–G366.
22. Galle, P.R., et al. 1995. Involvement of the CD95 (APO-1/Fas) receptor and ligand in liver damage. *J. Exp. Med.* **182**:1223–1230.
23. Kanzler, S., and Galle, P.R. 2000. Apoptosis and the liver. *Semin. Cancer Biol.* **10**:173–184.
24. Faubion, W.A., et al. 1999. Toxic bile salts induce rodent hepatocyte apoptosis via direct activation of Fas. *J. Clin. Invest.* **103**:137–145.
25. Bromberg, J., and Darnell, J.E. 2000. The role of STATs in transcriptional control and their impact on cellular function. *Oncogene.* **19**:2468–2473.
26. Ozaki, M., Suzuki, S., and Irani, K. 2002. Redox factor-1/APE suppresses oxidative stress by inhibiting the rac1 GTPase. *FASEB J.* **16**:889–890.
27. Yamakawa, Y., et al. 2000. Interaction of platelet activating factor, reactive oxygen species generated by xanthine oxidase, and leukocytes in the

generation of hepatic injury after shock/resuscitation. *Ann. Surg.* **231**:387–398.
28. Daemen, M.A.R.C., et al. 1999. Inhibition of apoptosis induced by ischemia-reperfusion prevents inflammation. *J. Clin. Invest.* **104**:541–549.
29. Yakar, S., et al. 1999. Normal growth and development in the absence of hepatic insulin-like growth factor I. *Proc. Natl. Acad. Sci. U. S. A.* **96**:7324–7329.
30. Ozaki, M., et al. 2000. Inhibition of the Rac1 GTPase protects against nonlethal ischemia/reperfusion-induced necrosis and apoptosis in vivo. *FASEB J.* **14**:418–429.
31. Grosch, S., Fritz, G., and Kaina, B. 1998. Apurinic endonuclease (Ref-1) is induced in mammalian cells by oxidative stress and involved in clastogenic adaptation. *Cancer Res.* **58**:4410–4416.
32. Grosch, S., and Kaina, B. 1999. Transcriptional activation of apurinic/apyrimidinic endonuclease (Ape, Ref-1) by oxidative stress requires CREB. *Biochem. Biophys. Res. Commun.* **261**:859–863.
33. Galun, E., Zeira, E., Pappo, O., Peters, M., and Rose-John, S. 2000. Liver regeneration induced by a designer human IL-6/sIL-6R fusion protein reverses severe hepatocellular injury. *FASEB J.* **14**:1979–1987.
34. Peters, M., et al. 2000. Combined interleukin 6 and soluble interleukin 6 receptor accelerates murine liver regeneration. *Gastroenterology.* **119**:1663–1671.
35. Hecht, N., et al. 2001. Hyper-IL-6 gene therapy reverses fulminant hepatic failure. *Mol. Ther.* **3**:683–687.
36. Malassagne, B., et al. 2001. The superoxide dismutase mimetic MnTBAP prevents Fas-induced acute liver failure in the mouse. *Gastroenterology.* **121**:1451–1459.
37. Suzuki, Y., Ono, Y., and Hirabayashi, Y. 1998. Rapid and specific reactive oxygen species generation via NADPH oxidase activation during Fas-mediated apoptosis. *FEBS Lett.* **425**:209–212.
38. Giardina, C., Boulares, H., and Inan, M.S. 1999. NSAIDs and butyrate sensitize a human colorectal cancer cell line to TNF-alpha and Fas ligation: the role of reactive oxygen species. *Biochim. Biophys. Acta.* **1448**:425–438.
39. Jayanthi, S., Ordonez, S., McCoy, M.T., and Cadet, J.L. 1999. Dual mechanism of Fas-induced cell death in neuroglioma cells: a role for reactive oxygen species. *Brain Res. Mol. Brain Res.* **72**:158–165.
40. Gulbins, E., et al. 1996. Fas-induced programmed cell death is mediated by a Ras-regulated O2- synthesis. *Immunology.* **89**:205–212.
41. Demple, B., Herman, T., and Chen, D. 1991. Cloning and expression of APE, the cDNA encoding the major human apurinic endonuclease: definition of family of DNA repair enzymes. *Proc. Natl. Acad. Sci. U. S. A.* **88**:11450–11454.
42. Mitomo, K., et al. 1994. Two different cellular redox systems regulate the DNA-binding activity of the p50 subunit of NF-kappa B in vitro. *Gene.* **145**:197–203.
43. Jayaraman, L., et al. 1997. Identification of redox/repair protein Ref-1 as a potent activator of p53. *Genes Dev.* **11**:558–570.
44. Huang, L.E., Arany, Z., Livingston, D.M., and Bunn, H.F. 1996. Activation of hypoxia-inducible transcription factor depends primarily upon redox-sensitive stabilization of its alpha subunit. *J. Biol. Chem.* **271**:32253–32259.
45. Nakamura, H., Nakamuta, K., and Yodoi, J. 1997. Redox regulation of cellular activation. *Annu. Rev. Immunol.* **15**:351–369.
46. Negoro, S., et al. 2001. Activation of signal transducer and activator of transcription 3 protects cardiomyocytes from hypoxia/reoxygenation-induced oxidative stress through the upregulation of manganese superoxide dismutase. *Circulation.* **104**:979–981.
47. Nakagami, H., et al. 2001. Mitogenic and antiapoptotic actions of hepatocyte growth factor through ERK, STAT3, and AKT in endothelial cells. *Hypertension.* **37**:581–586.
48. Ozaki, M., Haga, S., Zhang, H., Irani, K., and Suzuki, S. 2003. Inhibition of hypoxia/reoxygenation-induced oxidative stress in HGF-stimulated anti-apoptotic signaling: role of PI3-K and Akt kinase upon rac1. *Cell Death Differ.* **10**:508–515.
49. Ping, P., et al. 2002. Formation of protein kinase Cε-Lck signaling modules confers cardioprotection. *J. Clin. Invest.* **109**:499–507. doi:10.1172/JCI200213200.

ARTICLE

doi:10.1016/S1525-0016(03)00262-4

Improvement of Skeletal Lesions in Mice with Mucopolysaccharidosis Type VII by Neonatal Adenoviral Gene Transfer

Arihiko Kanaji,[1,2,3] Motomichi Kosuga,[1,3,4] Xiao-Kang Li,[1] Yasuyuki Fukuhara,[1,3,4] Akiko Tanabe,[1] Yuko Kamata,[1,3] Noriyuki Azuma,[1,3] Masao Yamada,[1] Toyonori Sakamaki,[2,3] Yoshiaki Toyama,[2] and Torayuki Okuyama[1,3,4,*]

[1]*National Research Institute of Child Health and Development, Tokyo 157-8535, Japan*
[2]*Department of Orthopedics and* [4]*Department of Pediatrics, Keio University School of Medicine, Tokyo 160-8582, Japan*
[3]*National Center for Child Health and Development, Tokyo 157-8535, Japan*

**To whom correspondence and reprint requests should be addressed at the Department of Clinical Genetics and Molecular Medicine, National Center for Child Health and Development, 2-10-1 Okura Setagaya-ku, Tokyo 157-8535, Japan. Fax: +81-3-3416-2222. E-mail: okuyama-t@ncchd.go.jp.*

Neonatal gene transfer using adenovirus vectors expressing human β-glucuronidase (AxCAhGUS) resulted in pathological improvement in multiple visceral organs of mice with mucopolysaccharidosis type VII (MPSVII). However, the therapeutic effect on skeletal deformities and growth retardation, the major clinical symptoms in MPSVII, was not fully investigated by biochemical and histopathological analyses. In this study, we injected AxCAhGUS into a murine model of MPSVII (B6/MPSVII) within 24 h of birth and evaluated the therapeutic effects on skeletal deformities and growth retardation. High levels of β-glucuronidase (GUSB) activity (approximately threefold higher than normal GUSB activity) were observed in the articular cartilage of the mice 30 days after the treatment. Histopathological study in the knee joints showed elimination of vacuole cells in the articular cartilage and growth plate. Subchondral bone near the articular surface was almost normal in the treated MPSVII mice. Long-term observation (for 140 days after treatment) indicated that characteristic phenotypes such as flattened face, hunched stature, and shortening of bone length in the treated mice were almost normal. These results demonstrate that a single injection of adenovirus vector into neonatal MPSVII mice is sufficient for long-term normalization of skeletal deformities and effective in pathological correction of the articular cartilage and growth plate.

Key Words: mucopolysaccharidosis, adenovirus, skeletal lesions, gene therapy

INTRODUCTION

Mucopolysaccharidosis type VII (MPSVII, Sly disease)is a lysosomal storage disease caused by a deficiency of β-glucuronidase (GUSB) activity, which results in a progressive accumulation of undegraded glycosaminoglycans in the lysosomes [1]. MPSVII is characterized pathologically by lysosomal distension in many tissues and clinically by hepatosplenomegaly, mental and growth retardation, hearing and vision defects, skeletal deformities, and short life span [2].

B6/MPSVII is a murine model of MPSVII, sharing characteristic phenotypes and pathological abnormalities with human MPSVII [3–5]. In this model, a single base pair deletion in exon 10 of the GUSB gene results in the formation of a premature stop codon, leading to the complete absence of GUSB activity [3].

B6/MPSVII is a useful model to develop novel therapeutic approaches, such as enzyme replacement therapy (ERT) and bone marrow transplantation (BMT) [6–12]. In adult MPSVII mice, ERT and BMT will reverse visceral lesions and prolong survival, but have little effect on growth retardation, bone dysplasia, or lysosomal storage in the central nervous system [6,7]. In contrast, neonatal MPSVII mice receiving ERT or BMT showed an improvement in skeletal deformities [7,11,12]. Sands *et al.* reported on the therapeutic effect of BMT on skeletal deformities during the neonatal period [11]. They showed pathological improvement of the articular surface, growth

1525-0016/03 $30.00

plate, and cortical bone in the treated MPSVII mice. Voglar *et al.* reported on the therapeutic effect of ERT on skeletal deformities during the neonatal period [12]. In their study, recombinant β-glucuronidase enzyme was administered intravenously into MPSVII mice at weekly intervals from birth to 6 weeks of age. Slight elimination of vacuolated osteocytes and osteoblasts was shown in the treated mice 14 days after the last injection of ERT. However, both BMT and ERT have limitations for the treatment of human MPSVII. For BMT, a shortage of suitable donors makes it difficult to apply widely. ERT requires frequent injections of the purified enzymes, which is very expensive in general. For these reasons, another treatment strategy has to be developed to improve skeletal deformities in MPSVII.

Recently, gene therapy for MPSVII including *in vivo* and *ex vivo* gene transduction approaches has been attempted using several viral vectors such as retroviruses [13–19], herpesviruses [20,21], adenoviruses [22–29], lentiviruses [30,31], and adeno-associated viruses [32–35]. Several types of cells, such as bone marrow cells [16], fibroblasts [17], and myoblasts [18], were transduced with retroviral vectors, and the cells overexpressing GUSB were administered into adult MPSVII mice locally as well as systemically. Limited correction of lysosomal storage in the liver and spleen was demonstrated following these *ex vivo* gene therapies. An *in vivo* gene therapy approach has also been successful for generating tissues overexpressing GUSB. We administered an E1/E3-deleted adenoviral vector expressing GUSB (AxCAhGUS) into MPSVII mice via the tail vein and demonstrated that high levels of GUSB were observed in the liver, spleen, kidney, lung, and heart [27].

We previously reported that intravenous administration of AxCAhGUS during the neonatal period was sufficient to improve facial and cranial bone deformities in mice with MPSVII [29]. Ponder *et al.* described remarkable improvement of skeletal-articular lesions in dogs with MPSVII after retroviral gene transfer shortly after birth [19]. Daly *et al.* also reported that AAV-mediated gene transfer during the neonatal period resulted in a remarkable improvement of characteristic phenotypes, such as flattered face, hunched stature, and shortening of bone length [35]. However, the therapeutic effect on skeletal deformities and growth retardation, the major symptoms in MPSVII, was not fully investigated by biochemical and histopathological analysis in these papers.

Here, we administered AxCAhGUS intravenously and evaluated the therapeutic effects on skeletal deformities and growth retardation in mice with MPSVII. These analyses demonstrate that the improvement of growth disturbance and pathological correction of the articular cartilage and growth plate are achievable by a single adenoviral administration into neonatal MPSVII mice.

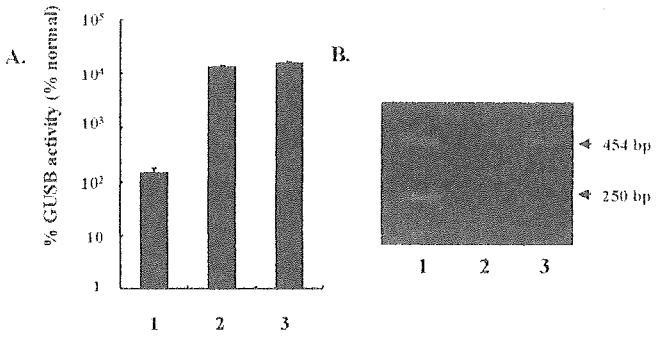

FIG. 1. Therapeutic efficacy in the articular cartilage of B6/MPSVII mice infected with AxCAhGUS in adulthood. (A) We injected 1.0 ml of viral solution containing 1×10^8 pfu of AxCAhGUS into adult B6/MPSVII mice (12–15 weeks of age). The mice were sacrificed 7 days after intravenous administration. The GUSB activities in the articular cartilage (lane 1), liver (lane 2), and serum (lane 3) were measured. Results are expressed as the percentage of GUSB activity found in the corresponding organs from four age-matched B6 (+/+) mice. (B) DNA from the articular cartilage and liver was extracted and used as templates for PCR. Virally encoded human GUSB cDNA in AxCAhGUS produced a 240-bp band, and the murine GUSB gene produced a 454-bp band. Both 454- and 240-bp DNA fragments were amplified when PCR was performed using DNA from the liver as templates, while a single 454-band was amplified by PCR using DNA from the articular cartilage as templates. In each group, four mice were used, and representative results are shown (lane 1, liver; lane 2, articular cartilage; lane 3, articular cartilage).

Results

Therapeutic Effect on Articular Cartilage of the MPSVII Mice Treated in Adulthood

To evaluate the therapeutic efficacy of adenovirus-mediated gene therapy on articular cartilage of MPSVII mice, we sacrificed the gene-transduced adult B6/MPSVII mice 7 days after intravenous administration of 1×10^8 plaque-forming units (pfu) of AxCAhGUS. We determined GUSB activity using 4-methylumbelliferyl β-D-glucuronide as substrate. We observed high levels of GUSB activity (1.5-fold higher than normal GUSB activity) in the articular cartilage (Fig. 1A, lane 1). In the liver, high levels of GUSB activity were also detected (Fig. 1A, lane 2). Moreover, to determine whether the origin of GUSB activity in the articular cartilage was due to transgene expression or due to cross-correction of lysosomal GUSB, we performed a PCR-based assay to detect virally encoded DNA in the articular cartilage. The PCR primers were designed based on the sequences of exon 6 and exon 7 of the human GUSB gene to amplify a 240-bp fragment from the human GUSB cDNA in the viral genome of AxCAhGUS. This PCR also generates a 454-bp fragment from the endogenous murine GUSB gene [27]. The 454-bp DNA fragment corresponding to the partial endogenous murine GUSB gene was amplified; however, the 240-bp partial human GUSB cDNA located in AxCAhGUS was not amplified (Fig. 1B) from the DNA of the articular cartilage, suggesting that GUSB detected in the articular cartilage was the result of

doi:10.1016/S1525-0016(03)00262-4

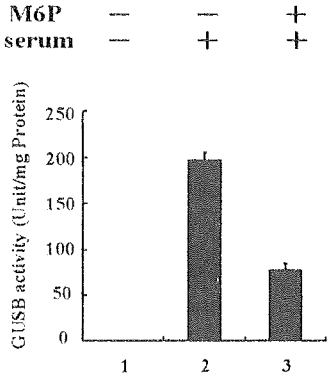

FIG. 2. Mannose 6-phosphate receptor-mediated endocytosis of GUSB in mouse chondrocytes. The articular cartilage from untreated MPSVII mice was incubated with medium with the serum from MPSVII mouse injected with 1×10^8 pfu of AxCAhGUS 7 days before. The serum contained 3.1×10^3 units of GUSB. The GUSB activity in the articular cartilage incubated with the serum was dramatically increased (lane 2); however, the increase was significantly suppressed when the articular cartilage was incubated in the presence of 6 mM mannose 6-phosphate (lane 3). The endogenous GUSB activity in the articular cartilage of MPSVII mice was negligible (lane 1).

in vivo cross-correction rather than direct gene transduction.

GUSB Cross-correction Mediated by the Mannose 6-phosphate Receptors in Chondrocytes

Cross-correction of many lysosomal enzymes is mediated mainly by the mannose 6-phosphate receptors expressed on cell surface membranes, and this process is efficiently blocked by mannose 6-phosphate [27]. To confirm that cross-correction mediated by mannose 6-phosphate receptors contributed to the high levels of GUSB activity in the articular cartilage of the treated MPSVII mice, we cocultured articular cartilage of the untreated MPSVII mice with medium containing serum obtained from the gene-transferred MPSVII mice. The GUSB activity was dramatically increased in the articular cartilage cocultured with serum containing 3.1×10^3 units of GUSB (Fig. 2, lane 2). Furthermore, the increase in GUSB activity was significantly reduced when 6 mM mannose 6-phosphate was present in the medium (Fig. 2, lane 3). These observations suggest that the GUSB enzyme was taken up by articular chondrocytes via the mannose 6-phosphate receptors.

Therapeutic Effects on Skeletal Deformities and Growth Retardation after Administration of AxCAhGUS during the Neonatal Period

Intravenous administration of AxCAhGUS in adulthood has little effect on growth retardation and skeletal deformities in MPSVII mice, because skeletal deformities and growth retardation are progressive from the neonatal period in mucopolysaccharidoses. To prevent skeletal deformities and growth retardation from progressing in MPSVII mice, we started treatment during the neonatal period. We injected 1×10^7 pfu of AxCAhGUS via the superficial temporal vein into the newborn MPSVII mice within 24 h of delivery and evaluated the therapeutic effect on skeletal deformities and growth retardation. Long-term observation (140 days after the treatment) demonstrated a remarkable improvement of growth retardation in the mice treated during the neonatal period (Fig. 3A2). The lengths of the tibia and fibula of the treated MPSVII mice were almost indistinguishable from those of their normal littermates (Fig. 3B2). These results demonstrate that morphological normalization of skeletal deformities in MPSVII is apparently achievable when the treatment starts during the neonatal period.

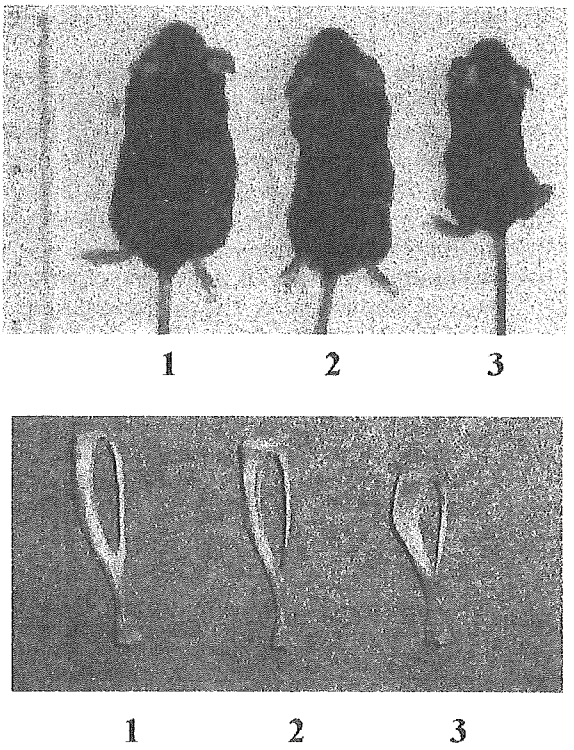

FIG. 3. Therapeutic effect on skeletal deformities and growth retardation in neonatally treated mice with MPSVII. (A) Growth retardation is a characteristic symptom of mice with B6/MPSVII. We injected 100 μl of viral solution containing 1×10^7 pfu of AxCAhGUS via the superficial temporal vein into neonatal B6/MPSVII mice within 24 h of delivery and evaluated the therapeutic effect on skeletal deformities and growth retardation 140 days after the treatment. The body length of the treated MPSVII mice (2) was indistinguishable from that of a B6 (+/+) littermate (1), while an untreated MPSVII littermate looked remarkably short (3). (B) The shape and length of the tibia and fibula of the neonatally treated mice (2) were compared with those of their affected (3) or normal (1) littermates. The long bones of the MPSVII mice (3) were significantly short and wide compared with those of their normal littermates (1), and the long bones of the treated MPSVII mice (2) show length and shape similar to those of their normal littermates.

Biochemical Analysis of Articular Cartilage in the Mice Treated during the Neonatal Period

To evaluate the therapeutic effect on skeletal deformities in more detail, we performed biochemical analysis. We sacrificed MPSVII mice treated during the neonatal period 30 days after the treatment and measured GUSB activities in the articular cartilage and liver (Figs. 4A and 4B). We observed high levels of GUSB activity (631.9 ± 69.9 unit/mg protein) corresponding to more than threefold higher than normal GUSB activity in the articular cartilage of the treated mice (Fig. 4A, lanes 1 and 2). In the liver, high levels of GUSB activity were also detected (Fig. 4A, lanes 3 and 4). We isolated chondrocytes from the articular cartilage of MPSVII mice and performed GUSB activity staining on the chondrocyte culture. About 40% of the chondrocytes from the MPSVII mice treated with AxCAhGUS were GUSB-positive cells (Fig. 4B). PCRs demonstrated that viral DNA was detectable in the articular cartilage of the MPSVII mice treated during the neonatal period (Fig. 4C). These results suggested that the articular cartilage was efficiently transduced with an adenoviral vector and extremely high levels of transgene expression could be obtained, when the mice were treated during the neonatal period.

Histopathological Analysis of Skeletal Lesions in the Mice Treated during the Neonatal Period

We compared histopathological analysis in the knee joint after the neonatal treatment (Figs. 5B, 5E, and 5H) with age-matched normal (Figs. 5A, 5D, and 5G) and untreated MPSVII mice (Figs. 5C, 5F, and 5I). Extensive vacuolization of the cells in the articular cartilage was not completely eliminated; however, they were obviously reduced in size and number after the treatment (Fig. 5B). The normal columnar architecture in the growth plate (resting zone, proliferative zone, hypertrophic zone, and endochondral; bone) was completely disrupted in the untreated MPSVII mice (Fig. 5F); however, we observed columnar architecture in the proliferative and hypertrophic zones in the MPSVII mice treated with neonatal gene therapy (Fig. 5E). Subchondral bone and bone marrow cells near the articular surface were significantly improved in the treated MPSVII mice (Fig. 5H). These results demonstrate that limited but significant improvement of pathological lesions in bone tissues was achieved in the gene-transduced MPSVII mice.

Discussion

Skeletal deformities and growth retardation are frequent manifestations of mucopolysaccharidoses. Multiple skeletal abnormalities, including short stature, angular deformities of the ribs, abnormally short forelimbs, subluxation of the hip joints, and epiphyseal dysplasia involving the vertebrae and long bones were observed in feline and murine models of MPSVII [4,36].

The pathogenesis of skeletal deformities and growth retardation was studied using several models of mucopolysaccharidoses [37,38]. Abreu *et al.* reported that clusters of distended chondrocytes disrupted the normal columnar architecture of the growth plate, presumably leading to bone growth abnormalities [37]. Simonaro *et al.* demonstrated that accumulated dermatan sulfate in the chondrocytes enhanced apoptosis of the articular cartilage cells in MPSVI cats, leading to degeneration of the articular surface [38]. These results suggest that abnormal chondrocytes in the articular cartilage and growth plate play an important role in skeletal deformities and growth retardation in mucopolysaccharidoses.

Recently, several reports have demonstrated that neonatal gene therapy contributed to a remarkable improvement of skeletal deformities in MPSVII mice [19,29,35]. However, histopathological and biochemical analyses of the skeletal lesions were not performed in these reports. Here, we demonstrated improvements in skeletal architecture and bone pathology in MPSVII mice by adenovirus-mediated gene therapy during the neonatal period.

Histopathological abnormality of the growth plate has been well characterized in other types of mucopolysaccharidoses [37,39]. Abreu *et al.* reported that poorly organized proliferative and hypertrophic zones were observed in the growth plate of MPSVI cats [37]. Silvery *et al.* also reported that the normal columnar architecture of the proliferative and hypertrophic zones was disrupted in the growth plate of a human patient with Hurler's syndrome [39]. In this study, almost total loss of the proliferative and hypertrophic zones was shown in the growth plate of untreated MPSVII mice, while a columnar architecture of the proliferative and hypertrophic zones was demonstrated in the growth plate of MPSVII mice following neonatal gene therapy. These results suggest that pathological improvement of the proliferating and hypertrophic zones in the growth plate is important for the normalization of growth retardation and bone development in MPSVII mice treated by neonatal gene transfer.

Moreover, biochemical analysis of the articular cartilage was performed following adult and neonatal gene therapy. When we injected adenoviral vectors into adult MPSVII mice, most of the vectors were distributed predominantly in the liver [27]. The GUSB enzyme was secreted mainly from hepatic cells and significantly taken up by other cells via the mannose 6-phosphate receptors expressed on the cell surface membrane. This pathway is called *in vivo* cross-correction. Our results demonstrated that this *in vivo* cross-correction mechanism also contributed to high levels of GUSB activity in the articular cartilage of the treated MPSVII mice following adult gene therapy. On the other hand, we previously reported that adenoviral vectors were distributed in multiple organs such as the liver, lung, heart, spleen, kidney, and brain in MPSVII mice treated by neonatal gene therapy [29]. In this study, a PCR-based method demonstrated that viral

doi:10.1016/S1525-0016(03)00262-4

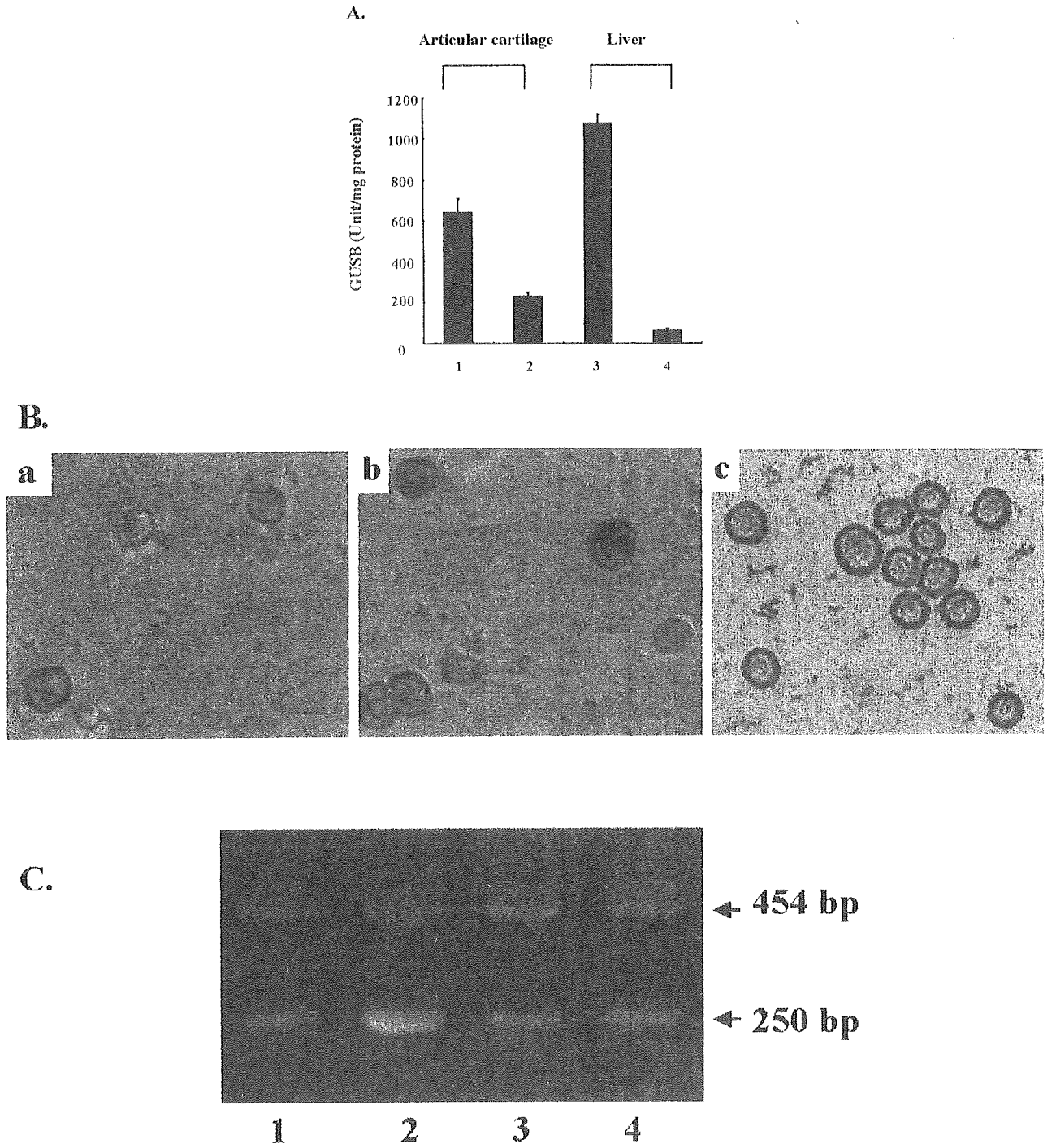

FIG. 4. Biochemical analysis of the articular cartilage of B6/MPSVII mice infected with AxCAhGUS in the neonatal period. (A) The mice treated during the neonatal period were sacrificed 30 days after the treatment and the GUSB activity in the articular cartilage and liver was measured. High levels of GUSB activity were observed in the articular cartilage (lane 1) and liver (lane 3) of the treated mice. (Lane 1, articular cartilage from the treated mice; lane 2, articular cartilage from normal B6 mice; lane 3, liver from the treated mice; lane 4, liver from normal B6 mice.) (B) Biochemical analysis with naphthol AS-BI β-*d*-glucuronide was also performed. Only GUSB-positive cells were observed in cells of B6 (+/+) mice (a). GUSB-positive chondrocytes (stained red) were identified in the treated MPSVII mice (b), while no GUSB-positive cells were observed in untreated MPSVII mice (c). (C) DNA from chondrocytes and livers was extracted and used as templates for PCR. Virally encoded human GUSB cDNA in AxCAhGUS generated a 240-bp band, and the murine GUSB gene produced a 454-bp band. Both the 240- and the 454-bp DNA fragments were amplified in both the articular cartilage and the liver. In each group, two mice were used for this experiment, and representative results are shown (lanes 1 and 2, liver; lane 3, articular cartilage; lane 4, articular cartilage).

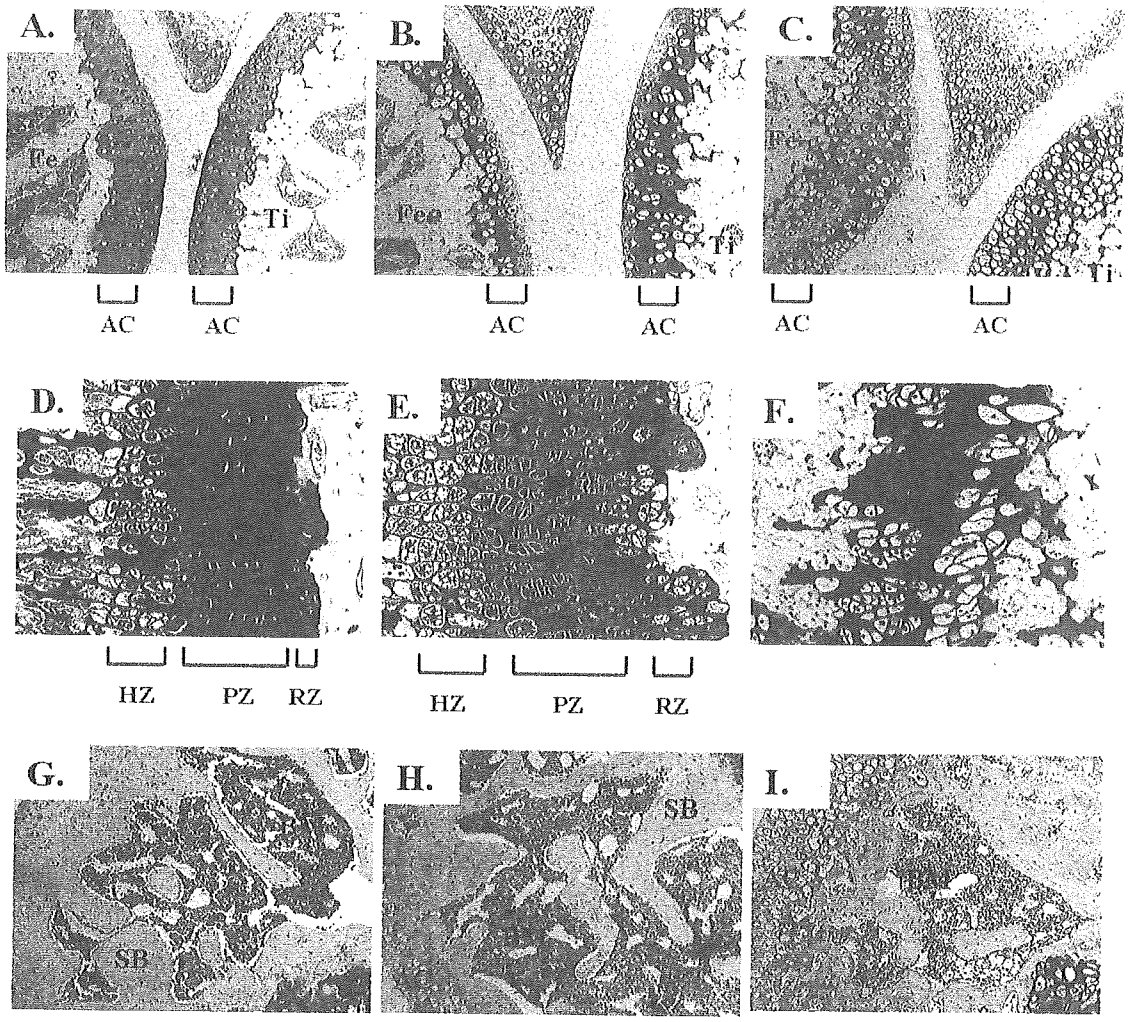

FIG. 5. Histopathological analysis of the epiphysis and metaphysis of the knee joint of B6/MPSVII mice treated with AxCAhGUS during the neonatal period. The mice that received adenoviral vectors during the neonatal period were sacrificed 30 days after the treatment, and pathological improvement in the articular cartilage and growth plate of the knee joint was evaluated. Toluidine blue staining of the epiphysis of normal mice (A), MPSVII mice 30 days after the treatment (B), and untreated MPSVII mice (C) is shown. Original magnification ×10. Moderate elimination of vacuole cells in the articular cartilage was observed in the treated mice with MPSVII. Toluidine blue staining of the metaphysis of normal mice (D), MPSVII mice 30 days after the treatment (E), and untreated MPSVII mice (F) is shown. Original magnification ×20. Moderate elimination of vacuole cells in the growth plate was also observed in the treated mice with MPSVII. Hematoxylin–eosin staining of the subchondral bone of normal mice (G), MPSVII mice 30 days after the treatment (H), and untreated MPSVII mice (I) is shown. Original magnification ×20. The subchondral bone near the articular surface was almost normal in the treated MPSVII mice. AC, articular cartilage; Fe, femur; Ti, tibia; GP, growth plate; RZ, resting zone; PZ, proliferative zone; HZ, hypertrophic zone; SB, subchondral bone; BM, bone marrow.

DNA was also detected in the articular cartilage after neonatal gene transfer. This result means that high levels of GUSB activity detected in the articular cartilage are not only due to *in vivo* cross-correction, but also due to transgene expression following neonatal gene therapy.

Successful *in vivo* gene transduction into murine articular chondrocytes during the neonatal period is the most important finding in this study. Gene transduction into the articular tissues has been already reported [40–42]. Arai *et al.* demonstrated *ex vivo* gene transduction into murine articular chondrocytes using adenoviral vectors [40]. In their study, efficient transgene expression was observed in the chondrocytes for at least 21 days. However, *in vivo* gene transduction into the articular chondrocytes was not successful when an intra-articular injection of viral vectors was carried out in adulthood [41,42].

There is a significant difference in the characterization of articular cartilage between adult and neonatal mice. The articular cartilage consists of sparse chondrocytes and a dense extracellular matrix. Each chondrocyte in the articular cartilage is isolated to its own lacuna and is surrounded by the extracellular matrix. The articular car-

doi:10.1016/S1525-0016(03)00262-4

tilage in adulthood is an avascular area and is nourished by synovial fluid diffusion. However, the articular cartilage during the neonatal period is adequately supplied with epiphyseal vessels [43]. When an intravenous administration of AxCAhGUS was given to neonatal MPSVII mice, the vector could transduce the articular chondrocytes via the artery.

To prevent the progression of skeletal deformity and growth retardation in MPSVII mice, persistent high levels of GUSB activity in the skeletal lesion should be maintained for at least 4 weeks after neonatal treatment, because the growth period of these mice is usually from birth to 4–8 weeks of age. In this paper, high levels of GUSB activity were observed in the articular cartilage 30 days after neonatal gene transfer. Moreover, we previously demonstrated the time-dependent change of serum GUSB activity in mice infected with AxCAhGUS during the neonatal period [29]. In that report, high levels of GUSB activity (10-fold higher than normal GUSB activity) were also observed in sera from treated mice 5 weeks after neonatal administration of AxCAhGUS. These results suggest that the persistent high levels of GUSB activity in MPSVII mice during the neonatal period are sufficient for not only histopathological improvement of articular cartilage and growth plate, but also remarkable improvement of growth retardation in MPSVII mice following neonatal gene therapy.

Here, we demonstrated the therapeutic effect on skeletal abnormalities using a murine model of MPSVII. It is important to prevent skeletal deformities from progressing in mucopolysaccharidoses and neonatal treatment is desirable for this purpose. Although several safety issues have to be resolved before clinical application, this neonatal gene therapy using an adenoviral vector is a promising strategy for treating the skeletal deformities of MPS-VII and other lysosomal storage diseases.

Materials and Methods

Generation of a recombinant adenovirus expressing human GUSB. An adenovirus, AxCAhGUS, for human GUSB was constructed by the COS-TPC method described previously [27]. A cosmid, AxCAhGUS, which contained an expression cassette of human GUSB under the control of the CAG promoter, was constructed by subcloning cDNA for human GUSB at a unique *Swa*I site of pAxCAwt. 293 cells were cotransfected with cosmid pAxCAhGUS and the adenovirus DNA–terminal protein complex, which had already been digested at several sites with *Eco*T22I. A recombinant adenovirus was generated through homologous recombination in the 293 cells.

Animals. Syngeneic B6 (+/+) and B6/MPSVII (mps/mps) mice were obtained from a pedigree colony of B6.C-H-2^{bml}/ByBir-gus^{mps}/+ maintained at the National Research Institute of Child Health and Development. All mice were maintained in accordance with the guidelines of the animal committee of the facility.

Quantitative analysis of GUSB in the articular cartilage and liver. The articular cartilage was removed from the bilateral patella, femoral head, and humeral head. The articular cartilage and liver were washed in Dulbecco's modified Eagle's medium (DMEM; Nissui Pharmaceutical, Tokyo, Japan). GUSB activities were measured in tissue homogenates using a fluorometric assay described previously [44]. Briefly, pellets were homogenized in 10 mM Tris–HCl (pH 7.5), 150 mM NaCl, 0.2% Triton X-100, and 1 mM dithiothreitol and centrifuged at 14,000 rpm for 1min to remove debris. The GUSB activities were measured using 4-methylumbelliferyl β-*d*-glucuronide (Sigma, St. Louis, MO) as substrate.

Isolation of chondrocytes from the articular cartilage and GUSB activity staining of the articular chondrocytes. Chondrocytes were isolated as previously described [40]. The articular cartilage was cut into pieces in DMEM supplemented with 10% fetal bone serum (FBS; Gibco BRL, Gaithersburg, MD), and treated with 0.025% collagenase and incubated at 37°C until the fragment was digested. Residual multicellular aggregates were removed by centrifugation, and cells were washed three times in DMEM, 5% FBS before the experiments. The chondrocytes were incubated in 24-well plates with a total volume of 1 ml of DMEM supplemented with 10% FBS for 2 days. GUSB activity staining was performed on the chondrocyte culture using naphthol AS-BI β-*d*-glucuronide (Sigma) as substrate, as previously described [27].

Detection of viral DNA in the articular cartilage. Total DNA of the tissue samples was extracted using a QIAamp DNA mini kit (Qiagen GmbH, Hilden, Germany) according to the manufacturer's protocol. Viral DNA of AxCAhGUS was detected using PCR to amplify the partial cDNA for human GUSB. The forward and reverse primers were synthesized based on the sequences of exon 6 (5′-CTGTGGCTGTCACCAAGAGC-3′) and exon 7 (5′-GGACACTCATCGATGACCAC-3′) of human GUSB cDNA. The sequences were identical to those of human cDNA, but had two mismatches within the murine exon 6 sequence. One hundred microliters of the PCR mixture contained 250 μM dNTPs, 10 pmol of the forward and reverse primers, 1 μg of purified DNA, and 2.5 U of *Taq* DNA polymerase (TaKaRa). Thirty cycles of PCR were carried out at 94°C for 90 s, 56°C for 90 s, and 72°C for 90 s. The expected products were a 240-bp fragment from cDNA and a 454-bp fragment from the endogenous murine gene.

Histopathology of the knee joints. Mice were sacrificed by cervical dislocation. Thereafter, the knee joints were removed and fixed in 10% formalin. After decalcification in 5% formic acid, the specimens were embedded in paraffin, sectioned at 5 μm, and stained with toluidine blue and hematoxylin–eosin. Histopathological sections were evaluated morphologically by light microscopy [40].

Acknowledgments

We thank Drs. Y. Kanegae and I. Saito for recombinant adenovirus constructs and Dr. J. Miyazaki for the CAG promoters. This work was supported in part by grants for Pediatric Research from the Ministry of Health, Labor, and Welfare, Japan, and by grants for Research on Health Sciences Focusing on Drug Innovation from the Japan Health Sciences Foundation.

RECEIVED FOR PUBLICATION MAY 27, 2003; ACCEPTED JULY 28, 2003.

References

1. Sly, W. S., Quinton, B. A., McAlister, W. H., and Rimoin, D. L. (1973). β-Glucuronidase deficiency: report of clinical, radiologic, and biochemical features of a new mucopolysaccharidosis. *J. Pediatr.* **82:** 249–257.
2. Birkenmeier, E. H., *et al.* (1989). Murine mucopolysaccharidosis type VII: characterization of a mouse with beta-glucuronidase deficiency. *J. Clin. Invest.* **83:** 1258–1266.
3. Sands, M. S., and Birkenmeier, E. H. (1993). A single-base-pair deletion in the beta-glucuronidase gene accounts for the phenotype of murine mucopolysaccharidosis type VII: a single-base-pair deletion in the beta-glucuronidase gene accounts for the phenotype of murine mucopolysaccharidosis type VII. *Proc. Natl. Acad. Sci. USA* **90:** 6567–6571.
4. Vogler, C., *et al.* (1990). A murine model of mucopolysaccharidosis VII: gross and microscopic findings in beta-glucuronidase-deficient mice. *Am. J. Pathol.* **136:** 207–217.
5. Sands, M. S., *et al.* (1997). Gene therapy for murine mucopolysaccharidosis type VII. *Neuromuscul. Disord.* **7:** 352–360.
6. Birkenmeier, E. H., *et al.* (1991). Increased life span and correction of metabolic defects in murine mucopolysaccharidosis type VII after syngeneic bone marrow transplantation. *Blood* **78:** 3081–3092.
7. Sands, M. S., *et al.* (1994). Enzyme replacement therapy for murine mucopolysaccharidosis type VII. *J. Clin. Invest.* **93:** 2324–2331.

8. Vogler, C., *et al.* (1997). Murine mucopolysaccharidosis type VII: long term therapeutic effects of enzyme replacement and enzyme replacement followed by bone marrow transplantation. *J. Clin. Invest.* **99:** 1596–1605.
9. Vogler, C., *et al.* (1999). Enzyme replacement in murine mucopolysaccharidosis type VII: neuronal and glial response to β-glucuronidase requires early initiation of enzyme replacement therapy. *Pediatr. Res.* **45:** 838–844.
10. O'Conner, L. H., *et al.* (1998). Enzyme replacement therapy for murine mucopolysaccharidosis type VII leads to improvement in behavior and auditory function. *J. Clin. Invest.* **101:** 1394–1400.
11. Sands, M. S., *et al.* (1993). Treatment of murine mucopolysaccharidosis type VII by syngeneic bone marrow transplantation in neonates. *Lab. Invest.* **68:** 676–686.
12. Vogler, C., Sands, M. S., Levy, B., Galvin, N. J., Birkenmeier, E. H., and Sly, W. S. (1999). Enzyme replacement with recombinant β-glucuronidase in murine mucopolysaccharidosis type VII: impact of therapy during the first six weeks of life on subsequent lysosomal storage, growth, and survival. *Pediatr. Res.* **45:** 838–844.
13. Gao, C., Sands, M. S., Harkins, M. E., and Ponder, K. P. (2000). Delivery of a retroviral vector expressing human β-glucuronidase to liver and spleen decreases lysosomal storage in mucopolysaccharidosis type VII mice. *Mol. Ther.* **2:** 233–244 , doi:10.1006/mthe.2000.0121..
14. Taylor, R. M., and Wolfe, J. H. (1997). Decreased lysosomal storage in the adult MPS VII mouse brain in the vicinity of grafts of retroviral vector-corrected fibroblasts secreting high levels of β-glucuronidase. *Nat. Med.* **3:** 771–774.
15. Taylor, R. M., and Wolfe, J. H. (1994). Cross-correction of β-glucuronidase deficiency by retroviral vector-mediated gene transfer. *Exp. Cell Res.* **214:** 606–613.
16. Marechal, V., Naffakh, N., Danos, O., and Heard, J. M. (1993). Disappearance of lysosomal storage in spleen and liver of mucopolysaccharidosis VII mice after transplantation of genetically modified bone marrow cells. *Blood* **84:** 1358–1365.
17. Moullier, P., Bohl, D., Heard, J. M., and Danos, O. (1993). Correction of lysosomal storage in the liver and spleen of MPSVII mice by implantation of genetically modified skin fibroblasts. *Nat. Genet.* **4:** 154–159.
18. Naffakh, N., Pinset, C., Montarras, D., Li, Z., Paulin, D., and Danos, O. (1996). Long-term secretion of therapeutic proteins from genetically modified skeletal muscles. *Hum. Gene Ther.* **7:** 11–21.
19. Ponder, K. P., *et al.* (2002). Therapeutic neonatal hepatic gene therapy in mucopolysaccharidosis VII dogs. *Proc. Natl. Acad. Sci. USA* **99:** 13102–13107.
20. Zhu, J., Kang, W., Wolfe, J. H., and Fraser, N. W. (2000). Significantly increased expression of beta-glucuronidase in the central nervous system of mucopolysaccharidosis type VII mice from the latency-associated transcript promoter in a nonpathogenic herpes simplex virus type 1 vector. *Mol. Ther.* **2:** 82–94, doi:10.1006/mthe.2000.0093.
21. Wolfe, J. H., Deshmane, S. L., and Fraser, N. W. (1992). Herpesvirus vector gene transfer and expression of β-glucuronidase in the central nervous system of MPS VII mice. *Nat. Genet.* **1:** 379–384.
22. Ghodsi, A., Stein, C., Derksen, T., Martins, I., Anderson, R. D., and Davidson, B. L. (1999). Systemic hyperosmolality improves β-glucuronidase distribution and pathology in murine MPS VII brain following intraventricular gene transfer. *Exp. Neurol.* **160:** 109–116.
23. Ghodsi, A., Stein, C., Derksen, T., Yang, G., Anderson, R. D., and Davidson, B. L. (1998). Extensive β-glucuronidase activity in murine central nervous system after adenovirus-mediated gene transfer to brain. *Hum. Gene Ther.* **9:** 2331–2340.
24. Ohashi, T., Watabe, K., Uehara, K., Sly, W. S., Vogler, C., and Eto, Y. (1997). Adenovirus-mediated gene transfer and expression of human beta-glucuronidase gene in the liver, spleen, and central nervous system in mucopolysaccharidosis type VII mice. *Proc. Natl. Acad. Sci. USA* **94:** 1287–1292.
25. Kosuga, M., *et al.* (2001). Engraftment of genetically engineered amniotic epithelial cells corrects lysosomal storage in multiple areas of the brain in mucopolysaccharidosis type VII mice. *Mol. Ther.* **3:** 139–148 , doi:10.1006/mthe.2000.0234..
26. Kosuga, M., *et al.* (2000). Phenotype correction in murine mucopolysaccharidosis type VII by transplantation of human amniotic epithelial cells after adenovirus-mediated gene transfer. *Cell Transplant.* **9:** 687–692.
27. Kosüga, M., *et al.* (2000). Adenovirus-mediated gene therapy for mucopolysaccharidosis VII: involvement of cross-correction in widespread distribution of the gene products and long-term effects of CTLA-4Ig coexpression. *Mol. Ther.* **1:** 406–413 , doi:10.1006/mthe.2000.0067..
28. Kamata, Y., *et al.* (2001). Adenovirus-mediated gene therapy for corneal clouding in mice with mucopolysaccharidosis type VII. *Mol. Ther.* **4:** 307–312 , doi:10.1006/mthe.2001.0461..
29. Kamata, Y., *et al.* (2003). Long-term normalization in the central nervous system, ocular manifestations, and skeletal deformities caused by a single systemic adenovirus injection into neonatal mice with mucopolysaccharidosis VII. *Gene Ther.* **10:** 406–414.
30. Stein, C. S., *et al.* (2001). In vivo treatment of hemophilia A and mucopolysaccharidosis type VII using nonprimate lentiviral vectors. *Mol. Ther.* **3:** 850–856 , doi:10.1006/mthe.2001.0325..
31. Bosch, A., Perret, E., Desmaris, N., Trono, D., and Heard, J. M. (2000). Reversal of pathology in the entire brain of mucopolysaccharidosis type VII mice after lentivirus-mediated gene transfer. *Hum. Gene Ther.* **11:** 1139–1150.
32. Sferra, T. J., *et al.* (2000). Recombinant adeno-associated virus-mediated correction of lysosomal storage within the central nervous system of the adult mucopolysaccharidosis type VII mouse. *Gene Ther.* **11:** 507–519.
33. Daly, T. M., Okuyama, T., Vogler, C., Haskins, M. E., Muzyczka, N., and Sands, M. S. (1999). Neonatal intramuscular injection with recombinant adeno-associated virus results in prolonged β-glucuronidase expression in situ and correction of liver pathology in mucopolysaccharidosis type VII mice. *Hum. Gene Ther.* **10:** 85–94.
34. Daly, T. M., Vogler, C., Levy, B., Haskins, M. E., and Sands, M. S. (1999). Neonatal gene transfer leads to widespread correction of pathology in a murine model of lysosomal storage disease. *Proc. Natl. Acad. Sci. USA* **96:** 2296–2300.
35. Daly, T. M., Ohlemiler, K. K., Roberts, M. S., Vogler, C., and Sands, M. S. (2001). Prevention of systemic clinical disease in MPSVII mice following AAV-mediated neonatal gene transfer. *Gene Ther.* **8:** 1292–1298.
36. Schultheiss, P. C., Gardner, S. A., Owens, J. M., Wenger, D. A., and Thrall, M. A. (2000). Mucopolysaccharidosis VII in a cat. *Vet. Pathol.* **37:** 502–505.
37. Abreu, S., *et al.* (1995). Growth plate pathology in feline mucopolysaccharidosis VI. *Calcif. Tissue Int.* **57:** 185–190.
38. Simonaro, C. M., Haskins, M. E., and Schuchman, E. H. (2001). Articular chondrocytes from animals with a dermatan sulfate storage disease undergo a high rate of apoptosis and release nitric oxide and inflammatory cytokines: a possible mechanism underlying degenerative joint disease in the mucopolysaccharidoses. *Lab. Invest.* **81:** 1319–1328.
39. Silveri, P., Kaplan, S., Fallon, D., Bayever, E., and August, S. (1991). Hurler syndrome with special reference to histologic abnormalities of the growth plate. *Clin. Orthop.* **269:** 305–311.
40. Arai, Y., *et al.* (1997). Adenovirus vector-mediated gene transduction to chondrocyte: in vitro evaluation of therapeutic efficacy of transforming growth factor-β1 and heat shock protein 70 gene transduction. *J. Rheumatol.* **24:** 1787–1795.
41. Watanabe, S., Imagawa, T., Boivin, G. P., Gao, G., Wilson, J., and Hirsch, R. (2000). Adeno-associated virus vector mediates gene transfer and delivery of chondroprotective IL-4 to murine synovium. *Mol. Ther.* **2:** 147–152 , doi:10.1006/mthe.2000.0111..
42. Gouze, E., *et al.* (2002). In vivo gene delivery to synovium by lentiviral vectors. *Mol. Ther.* **5:** 397–404.
43. Schiller, A. L. (1995). Pathology of Osteoarthritis: Osteoarthritic Disorder (In *K. E. Kunettner, and V. M. Goldgerg, Eds.), pp. 95–101. AAOS, Rosemont.*
44. Wolfe, J. H., and Sands, M. S. (1996). Murine mucopolysaccharidosis type VII: a model system for somatic gene therapy of the central nervous system. *Gene Transfer into Nervous System toward Gene Therapy of Neurological Disorders* (In *P. Lowenstain, and L. Enquist, Eds.), pp.263–274. Wiley, Essex, UK.*

Gene Therapy (2003) 10, 406–414

www.nature.com/gt

RESEARCH ARTICLE

Long-term normalization in the central nervous system, ocular manifestations, and skeletal deformities by a single systemic adenovirus injection into neonatal mice with mucopolysaccharidosis VII

Y Kamata[1,2], A Tanabe[1], A Kanaji[1], M Kosuga[1,2,3], Y Fukuhara[1,3], X-K Li[1], S Suzuki[1], M Yamada[1], N Azuma[1,2] and T Okuyama[1,2,3]

[1]*National Research Institute for Child Health and Development, Tokyo, Japan;* [2]*National Center for Child Health and Development, Japan; and;* [3]*Department of Pediatrics, Keio University School of Medicine, Japan*

Systemic injection of an adenovirus vector into adult mice resulted in pathological improvements in multiple visceral organs of mice with mucopolysaccharidosis VII; however, no therapeutic efficacy was observed for mental retardation, skeletal deformities, corneal clouding, and retinal degeneration. In this study, an adenovirus vector expressing human β-glucuronidase was injected into mice with mucopolysaccharidosis VII within 24 h of birth, and therapeutic efficacy was evaluated. In the brains of the mice, more than 20% of GUSB activity was maintained for at least 20 weeks after birth, and histopathological analysis showed no obvious lysosomal storage. Furthermore, no vacuolated cells were detected in corneal stroma and retinal pigment epithelium in the eyes of the mice treated in the neonatal period, while pathological improvement was not observed in adult MPSVII mice that received similar treatments. The treated mice also lacked characteristic facial skeletal deformities, and radiographic analysis demonstrated that their facial and cranial bones were morphologically normal. These results indicate that a single systemic adenovirus injection in the neonatal period could prevent the progression of mental retardation, corneal clouding, retinal degeneration, and skeletal deformities, all of which are frequently observed clinical manifestations and difficult to treat in adulthood.
Gene Therapy (2003) **10,** 406–414. doi:10.1038/sj.gt.3301869

Keywords: *mucopolysaccharidosis; gene therapy; adenovirus; neonatal treatment*

Introduction

Mucopolysaccharidosis type VII (MPSVII, Sly disease) is a lysosomal storage disease caused by a systemic deficiency of β-glucuronidase activity.[1] This defect results in a progressive accumulation of undegraded glycosaminoglycans (GAGs) in lysosomes, and affects multiple-tissues or organs simultaneously. B6/MPSVII is a murine model of MPSVII, sharing many pathological and clinical abnormalities with human MPSVII, and both phenotypic and genotypic similarities make this animal model suitable for evaluating novel therapeutic approaches to lysosomal storage disorders.[2–4]

The therapeutic efficacy of bone marrow transplantation (BMT) and enzyme replacement therapy (ERT) for MPSVII has been investigated intensively using the murine model B6/MPSVII,[5–9] and both therapies are in clinical trials. However, certian socioeconomic and clinical problems have prevented their widespread application. Namely, a shortage of suitable donors often prevents BMT, and the cost for enzyme production and necessity of frequent injection make ERT almost impractical.

As an alternative, gene therapy for MPSVII has been explored using several viral vectors such as retroviruses,[10–12] herpes viruses,[13,14] adenoviruses,[15–20] lentiviruses,[21,22] and adeno-associated viruses.[23–26] Both *in vivo* and *ex vivo* gene transduction methods have been tested experimentally; however, only limited therapeutic success has been reported, when studies were carried out using adult B6/MPSVII. Although it is clear that a more complete pathological correction can be obtained when ERT or BMT is started from the neonatal period, the efficacy of gene therapy for neonatal MPSVII has not yet been fully investigated.

Daly *et al* recently reported widespread pathological correction of B6/MPSVII by neonatal gene transfer using an adeno-associated viral (AAV) vector.[27–28] They generated an AAV vector for expressing human β-glucuronidase under the control of the CAG promoter (a combination of the chicken β-actin promoter and cytomegalovirus enhancer), and injected it into neonatal B6/MPSVII mice. They showed persistent pathological correction in the heart, brain, retina, and liver for at least 16 weeks. However, they also found comparatively low levels of the transgene GUSB activity in all organs following adeno-associated virus-mediated gene

Correspondence: T Okuyama, National Center for Child Health and Development, 2-10-1 Okura, Setagaya-Ku, Tokyo, 157-8535, Japan
Received 22 January 2002; accepted 16 June 2002

transfer. Even at an early time point (2–3 weeks after the treatment), only heart and liver had similar levels of GUSB activity to normal B6 mice, and in the other organs (lung, kidney, brain, and spleen), very little activity (less than 10% of that in normal mice) was detected. Moreover, marked decreases in GUSB activity were observed in the serum, liver, and spleen, and activity levels in all organs except the heart were less than 10% of those in normal mice at 16 weeks after birth. Although they showed sustained therapeutic levels of GUSB (1–5% of normal GUSB levels) in multiple tissues for a year in certain mice, it may be necessary to obtain more efficient transgene expression for the treatment of human MPSVII or other lysosomal storage diseases.

We previously reported the rapid elimination of lysosomal storage in multiple visceral organs of adult B6/MPSVII mice after intravenous administration of an adenovirus-expressing human GUSB.[20] When we injected the adenoviruses into B6/MPSVII via tail veins, they were distributed predominantly in the liver, and over-produced and secreted transgene products were delivered through the systemic circulation into the lung, heart, kidney, and spleen, and subsequent amelioration of lysosomal storage was observed. However, no GUSB expression was observed in the brain, suggesting that viral infection and GUSB transport were both prevented in the brain of adult mice presumably due to blood–brain barriers.

In this study, we administered the adenovirus to newborn B6/MPSVII or normal C3H mice and transgene expression and therapeutic efficacy were observed for 20 weeks. Persistently high levels of GUSB activity were observed for the 20 weeks, and a complete amelioration of lysosomal storage occurred in all organs examined including the brain, cornea, and retina, in the tissues of which, no or little pathological correction was observed in the mice treated in adulthood. We also showed effective secondary administration of adenoviral vectors in the mice treated during the neonatal period. Furthermore, morphological correction of facial and cranial bones was achieved by the neonatal adenoviral treatment.

Results

Distribution of GUSB activity in C3H mice treated with AxCAhGUS as newborns

Human β-glucuronidase (GUSB) is heat-stable, and was reduced by only 30% after 2-h incubation at 65°C. In contrast, the GUSB of C3H mice is heat-labile, and its activity is almost completely eliminated by the same treatment.[29] Using this difference of heat stability, we evaluated the gene transduction efficiency and distribution of the transgene products by infecting normal C3H mice with adenoviral vectors. Viral solution (100 μl) containing 1×10^7 plaque-forming units (pfu) of AxCAhGUS (an adenovirus-expressing human GUSB under the control of the CAG promoter) was injected into newborn C3H mice via superficial temporal veins. The mice were sacrificed periodically, and heat-stable GUSB activity was measured in liver, spleen, kidney, lung, heart, and brain (Figure 1). Since the endogenous GUSB level of C3H mice is approximately 10–40% of the GUSB level of

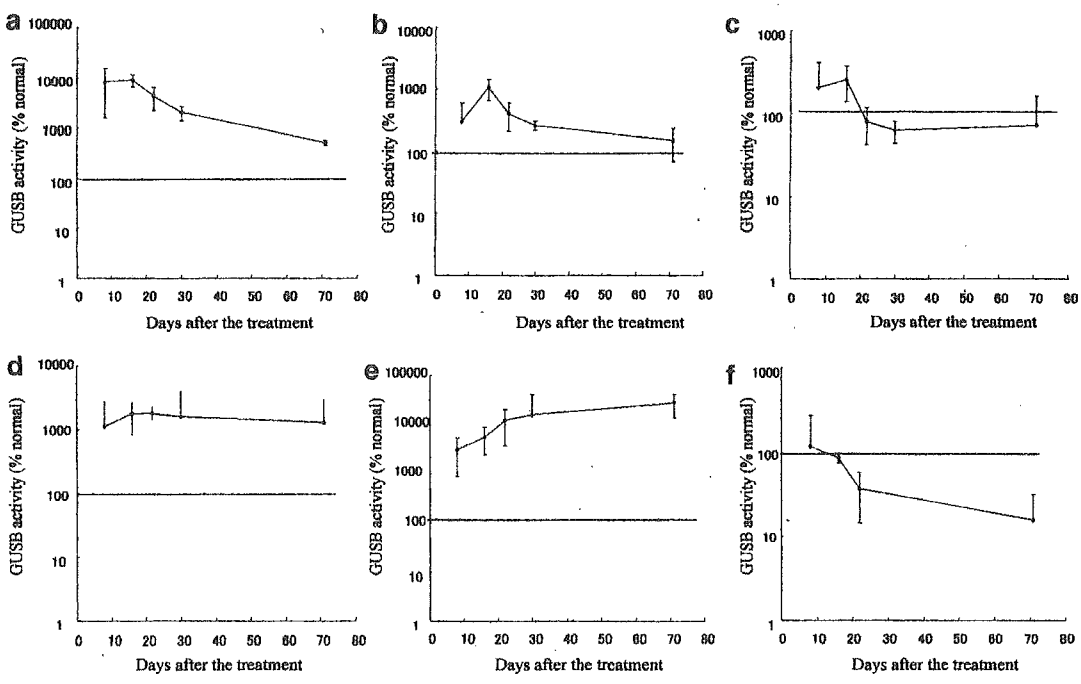

Figure 1 Time-dependent change of heat-stable β-glucuronidase (GUSB) activity in normal C3H mice infected with adenovirus-expressing human GUSB (AxCAhGUS). We injected 100 μl of viral solution containing 1×10^7 pfu of AxCAhGUS into newborn normal C3H mice within 24 h of delivery. The mice were sacrificed periodically, and heat-stable GUSB activity in each organ was measured. Each point represents the average and standard deviation for four treated animals. Results are expressed as a percentage of the GUSB activity found in the corresponding organs from four age-matched C57BL6 (B6) mice (a: liver; b: spleen; c: kidney; d: lung; e: heart; f: brain). Seven days after the treatment, high levels of the transgene activity (10–100 times higher than the GUSB activity of age-matched untreated B6 mice) were observed in liver (a), lung (d) and heart (e), while normal levels were detected in spleen (b), kidney (c) and brain (f). A time-dependent decrease of GUSB activity was observed in all examined organs, but more than 5% of the peak levels were still detected at 70 days after the treatment.

C57BL6 mice (B6 mice), we calculated '% normal activity' using GUSB level of age-matched normal B6 mice as 100%. Seven days after the treatment, high levels of the transgene (10–100 times the GUSB activity in age-matched normal B6 mice) were observed in liver, lung, and heart, while normal levels were detected in spleen, kidney, and brain (Figure 1). A time-dependent decrease of GUSB activity was observed in all examined organs, but more than 5% of the peak level was still detected even 70 days after the treatment.

Presence of viral DNA in C3H mice treated with AxCAhGUS

To determine whether the origin of the transgene GUSB in each organ is the result of transgene expression or due to cross-correction of lysosomal GUSB, viral DNA was detected with the PCR-based method (Figure 2). The PCR primers were designed based on the sequences of exons 6 and 7 of the human GUSB gene to amplify a 240-bp fragment from the human GUSB cDNA located in the viral genome of AxCAhGUS. This PCR also generates a 454-bp fragment from the endogenous murine GUSB gene.[20,30] When adult mice were infected with AxCAhGUS intravenously, a clear 240-bp DNA fragment was only detected in the PCR reaction from liver DNA, suggesting that AxCAhGUS accumulated predominantly in the liver. On the other hand, clear 240-bp DNA fragments were observed in all organs, when AxCAhGUS was intravenously administered into newborn mice, demonstrating that a significant amount of virus was distributed into multiple organs including the brain. These results indicate that the GUSB activity detected in extra-hepatic organs of the treated adult mice was due to cross-correction of a lysosomal enzyme rather than direct gene transduction; however, direct gene transduction also significantly contributed to GUSB expression in extra-hepatic organs in the mice treated as newborns.

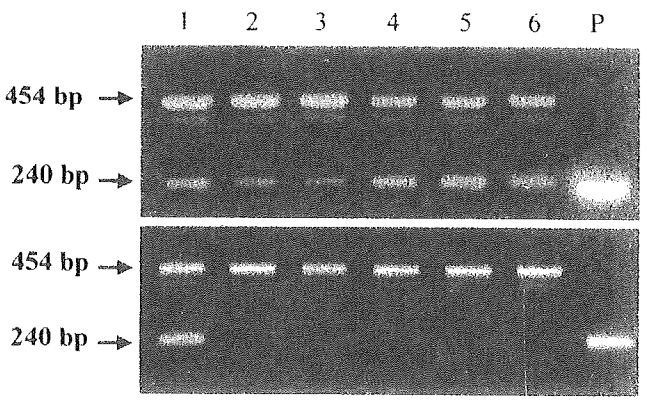

Figure 2 Detection of virally encoded human GUSB cDNA in mice treated with AxCAhGUS. We injected AxCAhGUS into C3H mice within 24 h of delivery or 30–40 days after birth. Seven days after the treatment, the mice were sacrificed and DNA from several organs was extracted and used as template for PCR. Virally encoded human GUSB cDNA in AxCAhGUS produces a 240-bp band, and the murine GUSB gene produces a 454-bp band. An intense 240-bp band was identified in all organs examined including the brain in the mice treated in the neonatal period (a), while the corresponding band was identified only in the liver in the mice treated at the age of 30–40 days. In each group, four mice were used for this experiment, and representative results are shown. Lane 1: liver; lane 2: spleen; lane 3: kidney, lane 4: lung; lane 5: heart; lane 6: brain. Lane P shows the result of the PCR reaction using human GUSB cDNA as a template.

Therapeutic efficacy of neonatal gene therapy in visceral organs

We injected an adenovirus 'AxCAhGUS' into four newborn B6/MPSVII mice and measured GUSB activity in visceral organs 30 days later. Higher than normal levels of GUSB activity (1–50 times higher than normal) were observed in liver, spleen, lung, and heart; approximately half of the normal activity was observed in kidney (Figure 3A). Histochemical study showed disseminated GUSB-positive cells in all visceral organs, which agreed with the result of the quantification of GUSB activity (data not shown). Furthermore, histopathological analysis demonstrated complete morphological normalization in liver and spleen in the mice treated during the neonatal period (Figure 3B).

Therapeutic efficacy of neonatal gene therapy in CNS lesions

We previously showed that the intravenous administration of AxCAhGUS into adult mice resulted in significant

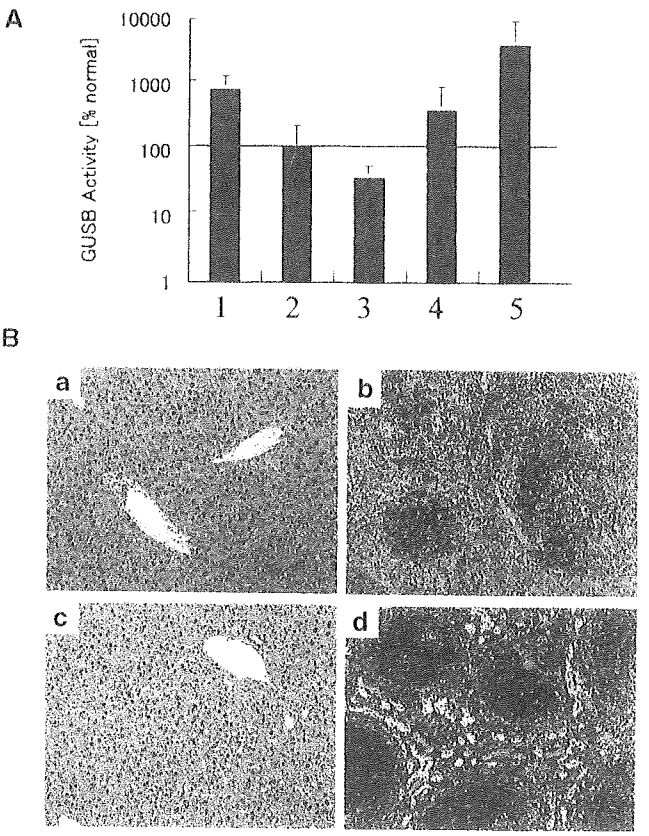

Figure 3 Therapeutic efficacy in visceral organs of B6/MPSVII mice infected with AxCAhGUS in the neonatal period. (A) We injected 100 μl of viral solution containing 1×10^{7} pfu of AxCAhGUS into newborn B6/MPSVII mice within 24 h of delivery. The mice were sacrificed 30 days after the treatment and GUSB activity in each organ was measured. Each point represents the average and standard deviation for four treated animals. Results are expressed as a percentage of GUSB activity found in corresponding organs from six age-matched B6 (+/+) mice (lane 1: liver; lane 2: spleen; lane 3: kidney; lane 4: lung; lane 5: heart). (B) Histopathological study shows complete elimination of lysosome storage in liver (a) and spleen (b). For comparison, toluidine blue staining of liver (c) and spleen (d) of age-matched untreated B6/MPSVII mice is shown.